Contamination of MORB by anatexis of magma chamber roof rocks: constraints from a geochemical study of experimental melts and associated residues

Lydéric France[a],*; Juergen Koepke[b]; Christopher J. MacLeod[c]; Benoit Ildefonse[d]; Marguerite Godard[d]; Etienne Deloule[a]

[a] CRPG; UMR 7358, CNRS; Université de Lorraine, 15 rue Notre Dame des Pauvres, 54501 Vandœuvre-lès-Nancy, France

[b] Institut fuer Mineralogie, Universitaet Hannover, Callinstrasse 3, 30167 Hannover, Germany

[c] School of Earth & Ocean Sciences, Cardiff University, Main Building, Park Place, Cardiff CF10 3AT, UK

[d] Géosciences Montpellier, CNRS, Université Montpellier 2, CC 60, 34095 Montpellier cedex 05, France

*corresponding author: lyde@crpg.cnrs-nancy.fr

Abstract

Mid-ocean ridge basalts (MORB) are the most abundant magmas produced on Earth. They are widely studied to infer mantle compositions and melting processes. However, MORB liquids are also the complex end-product of a variety of intra-crustal processes such as partial or fractional crystallization, melt-rock interaction, and contamination. Deciphering the relative contribution of these different processes is of first-order importance. Contamination at ocean crustal levels is likely, and may occur at magma chamber margins where fresh magmas can interact with previously hydrothermally altered rocks. Characterizing the composition of this crustal contaminant component is critical if we are to understand the relative importance of each component in the resulting MORB liquid.

Here we present the results of experiments designed to reproduce the processes occurring at oceanic magma chamber roofs, where crustal contamination should be most extensive, by melting a representative sample of the sheeted dike complex. Anatectic melts thus produced are likely to represent the principal crustal contaminant in MORB. These melts were characterized for major and trace elements, showing B, Zr, Hf, U enrichment, and Sr, Ti, V depletion relative to original MORB liquids. In comparison to the starting material, relative element fractionations are observed in the anatectic melts, with enrichments of: U relative to Ba, Nb, and Th; LREE and MREE relative to Sr; and Zr-Hf relative to LREE. Bulk partition coefficients for element partitioning during magma chamber roof anatexis are derived, and proposed as valuable tools for tracking MORB contamination.

Comparison with natural samples from the East Pacific Rise and the Oman ophiolite shows that anatectic melts can crystallize *in situ* to form oceanic plagiogranite intrusions, and that residual assemblages associated with the hydrous partial melting stage are represented by hornfelsic dikes and enclaves (also named granoblastic basalts). We now recognize these as commonplace at the root of the sheeted dike complex both at present-day and fossil oceanic spreading centers.

1. Introduction

Magmatism at mid-ocean ridges represents the largest igneous process on Earth, and plays a key role in global geodynamic cycles, from mantle melting to lithosphere recycling via subduction zones. The bulk composition of the hydrothermally altered oceanic crust is utilized in attempts to quantify chemical and isotopic cycles within the mantle (e.g., Hofmann and White, 1982; Alt et al., 1986; Moreira et al., 2003). That of Mid-Ocean Ridge Basalts (MORB), the shallowest manifestation of this magmatism, is commonly utilized to assess mantle composition and heterogeneities, melting parameters (e.g., Rubin et al., 2009), crustal thermal structure (e.g., Rubin and Sinton, 2007) and/or thickness (e.g., Klein and Langmuir, 1987). Nevertheless, before reaching the seafloor, MORB are likely to experience a suite of crustal processes: not simply partial or fractional crystallization but also reactive melt migration during porous flow, replenishment, and contamination/interaction with sea water and hydrothermally altered components, all of which have the potential to skew the mantle chemical signal in the resultant liquid (e.g., Grove et al., 1992; Coogan et al., 2003; Klein, 2003; Lissenberg and Dick, 2008; France et al., 2009a, 2013; Koepke et al., 2011; O'Neill and Jenner, 2012; Lissenberg et al., 2013).

At fast spreading ridges, the magmatic system is composed of a thick crystal mush (hereinafter referred to as 'the main magma chamber') containing only a few percent of melt (probably much less than 20%, e.g., Caress and Burnett, 1992; Crawford et al., 1999; Lamoureux et al., 1999; Dunn et al., 2000), overlain at the top of the lower crust by a thin (~50-100 m) and narrow (~1000 m) melt lens filled predominantly with melt (Figure 1a, e.g., Morton and Sleep, 1985; Detrick et al., 1987). This sub-axial melt lens feeds an upper crust formed of dikes and lavas (Sinton and Detrick, 1992; Singh et al., 1998; MacLeod and Yaouancq, 2000; Einaudi et al., 2003; France et al., 2009a; Koepke et al., 2011; Wanless and Shaw, 2012). All processes occurring within and around this melt lens will influence MORB composition.

Partial or fractional crystallization, reactive melt flow, and replenishment cycles are commonly considered as being the principal processes modifying the chemical signal of MORB (e.g., Grove et al., 1992; Klein, 2003; O'Neill and Jenner, 2012; Lissenberg et al., 2013). Nevertheless, some authors have presented evidence that a contaminating component is involved at various oceanic sites, either in present day oceanic crust (Michael and Schilling, 1989; Chaussidon and Marty, 1995; Michael and Cornell, 1998; Haase et al., 2005; Le Roux

et al., 2006; Wanless et al., 2010; France et al., 2009a; Koepke et al., 2011), or in ophiolites (Gillis and Coogan, 2002; Coogan, 2003; Coogan et al., 2003; Gillis et al., 2003; France et al., 2009a, 2013). Contamination of MORB may occur during seafloor eruptions through interaction with seawater (e.g., Michael and Schilling, 1989), or at magma chamber margins where fresh MORB may interact with hydrothermally altered crust (Gillis and Coogan, 2002; France et al., 2009a, 2013; Wanless et al., 2010; Koepke et al., 2011). Detailed studies performed at the East Pacific Rise (EPR), and in the Oman and Troodos (Cyprus) ophiolites have shown that the melt lens is a dynamic horizon that can migrate up and down with the potential to reheat, assimilate, and possibly re-melt the previously hydrothermally altered dikes (Figure 1b; Pedersen, 1986; MacLeod and Rothery, 1992; Hooft et al., 1997; Coogan et al., 2003; Gillis, 2008; Wilson et al., 2006; France et al., 2009a, 2010, 2013; Koepke et al., 2011). Reheating and assimilation can be associated with dehydration and/or hydrous partial melting of the previously altered rocks and thus can trigger contamination of the melt lens; it is therefore likely to represent the principal crustal contaminant in MORB (Figure 1; Pedersen and Malpas, 1984; Coogan et al., 2003; France et al., 2009a, 2013; Koepke et al., 2011). Small but ubiquitous leucocratic or felsic intrusions (often termed 'oceanic plagiogranites', see Koepke et al., 2007 for a review of this term) observed close to oceanic magma chamber roofs also attest to the crystallization of such anatectic melts (Figure 2a; e.g., Pedersen and Malpas, 1984; Gillis and Coogan, 2002; Coogan et al., 2003; Rollinson, 2009; France et al., 2010; Grimes et al., 2013), although oceanic plagiogranites can also be produced by extreme fractionation of MORB melts (e.g., Pedersen and Malpas, 1984; Berndt et al., 2005; Rollinson, 2009; Grimes et al., 2011). To date, oceanic plagiogranites have mostly been recognized from the sheeted dike / gabbro transition of ophiolites. In present day oceanic crust this transition has only been sampled sparsely in three locations (ODP Hole 1256D, Pito Deep and Hess Deep), at two of which the equivalent lithologies have been recognized in the form of small silica rich veinlets. The genesis of those anatectic melts is associated with the formation of a companion residual assemblage, consisting mostly of plagioclase, clinopyroxene, orthopyroxene, and oxides: hornfelses with a characteristic granoblastic texture (Figure 1b, 2b). Corresponding rocks are recognized in present day oceanic crust (Wilson et al., 2006; Gillis, 2008; Koepke et al., 2008; France et al., 2009a; Marks et al., 2011; Teagle et al., 2012) and in the ophiolites of Norway, Oman and Troodos (Pedersen and Malpas, 1984; Pedersen, 1986; Coogan et al., 2003; Gillis et al., 2008; France et al., 2009a). In past studies, they were variously termed granoblastic dikes / basalts (Wilson et al., 2006; Gillis, 2008; Koepke et al., 2008; France et al., 2009a, 2010; Teagle et al., 2012), hornfelsic

residues (Gillis, 2002, 2008), or recrystallized dikes (Coogan et al., 2003; Wilson et al., 2006). Those residual assemblages are also alternatively interpreted as pure metamorphic dehydrated lithologies (e.g., Gillis and Roberts, 1999; Wilson et al., 2006; France et al., 2010). Hornfels, their original name (Gillis and Roberts, 1999), will be used hereinafter to describe these lithologies. At fast spreading ridges, hornfelses are recovered within the root zone of the sheeted dike complex over a distance of some tens of meters away from the dike-gabbro boundary (Figure 1; e.g., Coogan et al., 2003; Wilson et al., 2006; Gillis, 2008; Koepke et al., 2008; France et al., 2009a), and should therefore be regarded as part of the main suite of lithologies that forms the oceanic crust. Numerous hornfels xenoliths are also observed within the horizon of isotropic gabbros that are thought to result from the crystallization of the melt lens (Figure 1; Wilson et al., 2006; Gillis, 2008; Koepke et al., 2008, 2011; France et al., 2009a, 2010).

Determining the composition of the anatectic melt and of the associated residual hornfels is key to (*i*) identifying those lithologies in natural settings, (*ii*) identifying and tracking the crustal contamination component in MORB, (*iii*) and improving our knowledge of chemical budgets in the oceanic crust.

In order to simulate the natural processes of partial melting and assimilation France et al., (2010) conducted partial melting experiments of dikes sampled from the Oman ophiolite. These dikes are considered to be representative of the hydrothermally altered roofs of fast spreading ridge magma chambers. France et al., (2010) documented the phase assemblages and major element compositions of experimental melts and residual crystals and compared them with natural examples of anatectic melts and associated residual hornfels assemblages from recent oceans and ophiolites. They demonstrated that: (*i*) the melts thus generated are of calc-alkaline character (Figure 3); (*ii*) the melts have compositions matching those of numerous oceanic plagiogranites (Figure 3); and (*iii*) residual assemblages are similar to natural hornfels.

A limitation of France et al. (2010)'s study was that trace elements were not analyzed in the experimental products. Recent work has, however, shown that trace elements are in many respects far more sensitive than major elements in constraining details magma chamber processes (e.g., Klein, 2003; O'Neill and Jenner, 2012; Lissenberg et al., 2013). Accordingly, in the current paper we present trace element analyses of the experimental products of France et al. (2010), and compare them to compositions of natural samples from the EPR (IODP

Hole 1256D) and the Oman ophiolite. The new results are used to discuss key processes occurring within oceanic magma chambers, and to quantify the composition of the principal MORB crustal contaminant.

2. Experimental and analytical techniques

Hydrous partial melting experiments were performed using a representative sample of hydrothermally altered dikes as a starting material: a fully altered basaltic dike (08OL30) from the Aswad area (Sumail massif) of the Oman ophiolite. Details of experimental conditions and starting material are given in France et al. (2010), but the main characteristics of the experimental setup are summarized here.

After crushing in a homemade stainless steel mortar, three fractions (30-100 µm, 100-150 µm, and 150-250 µm) were used in a preliminary experiment to control the effect of grain size on the experimental results. No effect of the starting material grain size on resultant chemistry was identified (France et al., 2010). For the experiments, the 150-250 µm fraction was used for trace element measurements, as it allowed us to obtain the largest melt pools. Conditions were chosen to match those prevailing at the base of the sheeted dike complex: pressure was 100 MPa, oxygen fugacity varied between FMQ+1.2 and +1.6 (where FMQ is the fayalite-magnetite-quartz oxygen buffer equilibrium), in agreement with results on natural samples (Koepke et al., 2008; France et al.; 2009a, 2010), and temperature ranged from 850 to 1030°C. Because of the presence of strongly hydrated phases in the starting material, all experiments were water-saturated. That water saturation was achieved is confirmed by the systematic occurrence of bubbles in anatectic melts.

Major and trace element concentrations of starting materials, and of EPR samples (hornfelses from IODP Hole 1256D; see Table A1 for sample localities) were determined by ICP-OES and ICP-MS, respectively at the Service d'Analyse des Roches et des Minéraux (SARM, CRPG, France). Analyzes were performed using HNO_3 solutions prepared from fused glass. Details of sample preparation, analytical settings and conditions, and detection limits, are given in Carignan et al. (2001). Analytical uncertainties are 2% for major elements, and 5 to 10% for trace element concentrations.

Major and trace element abundances of Oman ophiolite samples (dikes and hornfelses from Wadi Abyad; see Table A1 for sample localities and petrological information) were determined at Cardiff University using a JobinYvon Horiba Ultima 2 ICP-OES, and a ThermoElemental X7 ICP-MS equipped with a Cetac AS-500 autosampler, respectively. For major elements, ~2g of sample was ignited in a furnace at 900°C to drive off volatiles and determine loss on ignition values. Samples were then dissolved using the lithium metaborate fluxy-fusion dissolution method outlined in McDonald and Viljoen (2006). For trace elements, 200 mg of each sample were dissolved in concentrated HF on a hotplate (100°C) in a Teflon pot for the night, evaporated down and re-dissolved in concentrated HNO_3, and left on a hot plate one more night. The obtained solution was then evaporated to dryness; the resulting powder was taken up in 5 ml of 5 M HNO_3 prior to dilution with deionized water to a final volume of 50 ml. Calibration was against international rock standards (BIR and BEN), and prepared in the same way as the samples.

Major element compositions of experimental melts were obtained using a Cameca SX100 electron microprobe (Institüt für Mineralogie, Hannover) equipped with 5 spectrometers, utilizing 'Peak sight' software. All analyses were performed using a 15kV acceleration potential, a static (fixed) beam, Kα emission from all elements. The matrix correction was based on Pouchou and Pichoir (1991). Analyses of glasses were performed with a beam current set to 2 to 6 nA to minimize migration and volatilization of the alkali elements. Cl was analyzed subsequently using a beam current of 20 nA. Counting time was from 2 to 5 s for Na and K and from 5 to 10 for other elements (Si, Ti, Al, Mg, Fe, Ca, Mn, Cr, Cl). In the experiments where melt pools were large enough, the beam was defocused to a spot size of 5 to 20μm.

When large melt pools were available, trace element analyses of experimental melts were performed at the Géosciences Montpellier lab (Service Inter-régional Microsonde Sud, Montpellier, France) using a modified Cameca IMS4f ion probe. Polished sections of the experimental results were carbon-coated. A 15 kV O$^-$ primary beam was used with a 10 nA intensity and a beam size of ~25μm. The positive secondary ion were accelerated with a 4.5 kV voltage, and analyzed with a mass resolving power of 500, and an energy offset of -80V with a 30eV energy window in order to minimize the matrix effect. Each analysis consists of 10 cycles starting from 25.7 mass (used as background and for magnet adjustment), then ^{30}Si (2 s), ^{45}Sc (2 s), ^{47}Ti (2 s), ^{51}V (2 s), ^{88}Sr (2 s), ^{89}Y (2 s), ^{90}Zr (2 s), ^{93}Nb (10 s), ^{137}Ba (10 s),

^{180}Hf (20 s), ^{232}Th (30 s), ^{238}U (30 s) and almost all the rare earth isotopes (10 s) (counting time in brackets). The counting time is 30 s for Eu and 20 s for Lu. The data were corrected for oxide interferences (e.g., Fahey et al., 1987). ^{30}Si was used as the reference mass, though we found that the choice of reference element introduced no systematic offset in the results. The calibration factor was determined from the measurement of NIST 610 (Reed, 1992; Pearce et al., 1997) at the beginning and the end of each analytical session. Typical error on the samples (1 sigma error of mean: $\sigma/\sqrt{n}$, n = number of cycles) is less than 15% for all trace elements, except for Tb, Er, Lu, Hf (<17.5%), Th (23%) and U (32%). Signal stability was also carefully monitored for every analysis. All pits were checked using SEM imaging after analyses to ensure that only melts were analyzed.

Li-Be-B concentrations of experimental melts were determined using a Cameca IMS-1270 ion probe at CRPG (Nancy, France). Polished sections of the experimental results were carbon-coated. A 13 kV O$^-$ primary beam was used with a 20 nA intensity and a projected beam size of 20 μm. The positive secondary ion were accelerated with a 10 kV voltage, and analyzed with a mass resolving power of 1500. An energy offset of -40V with a 30eV energy window was used to minimize the matrix effect. Each analysis consists of 30 cycles starting from 6.8 mass (used as background and for magnet adjustment, measured during 4 s), then ^{7}Li (8 s), ^{9}Be (8 s), ^{11}B (8 s), ^{30}Si (4 s) (counting time in brackets). To prevent surface contamination, the 10 first cycles were not considered. Again, ^{30}Si was used as the reference mass. The calibration factor was determined from the measurement of GB4 standard (a silicate glass classically used as the CRPG internal standard for Li, Be, B measurements) at the beginning and the end of each analytical session. Data validity was checked by analyzing UTR2, NBS614 and NBS617 standards as unknown (UTR-2 glass from Stix and Layne, 1996). Typical error on the samples is around 15% for Li, Be, B. Signal stability was also carefully monitored for every analysis. All pits were checked using SEM imaging after analyses to ensure that only melts were analyzed.

3. Results

3.1. Experimental starting material and products

The starting material (dike sample 08OL30 from the Aswad area of the Oman ophiolite) composition is characteristic of the Oman ophiolite basalts (Tables 1, 2; France et al., 2010).

It is close to the composition of a typical altered EPR basalt (slightly enriched in Na, and depleted in Ca, and Mn relative to N-MORB; Figure 4), and is here considered as representative of the hydrothermally altered rocks forming the sheeted dike complex at fast spreading ridges. 08OL30 has a Mg# of 49 (with Mg#=Mg/(Mg+Fe)*100 in molar proportions), a SiO_2 content of 54.1 wt %, a TiO_2 content of 1.5 wt %, and a Na_2O content of 4.8 wt % (recalculated anhydrous; Table 1). Experimental anatectic melt compositions (Table 1; Figure 4) vary from 55.5 to 72.6 SiO_2 wt %, with decreasing partial melting fraction from 93 to 1 % (i.e., when temperature decreases from 1030 to 850°C). With decreasing amount of partial melting, MgO varies from 3.7 to 0.25 wt %, FeO from 8.9 to 1.6 wt %, Al_2O_3 from 17.25 to 16.5 wt %, TiO_2 from 1.5 to 0.3, K_2O from 0.2 to 2.2, and Mg# from 42.2 to 21.6. Water content was determined by France et al. (2010) to be 4.8 wt % in the 1030°C experiment. Major element compositions of anatectic melts have been shown to be in the range of oceanic plagiogranites (Figure 3), highlighting that hydrous partial melting of previously hydrothermally altered dikes has the potential to produce oceanic felsic rocks (France et al., 2010). Residual assemblages are multi-mineral assemblages and their bulk composition cannot be analyzed directly. Nevertheless, they can be calculated by using the starting material whole rock composition and the melt composition, using the mass balance equation (1).

(1) $[concentration]_{starting\ material} = x\ [concentration]_{melt} + (1-x)\ [concentration]_{residue}$,

where x is the melt fraction. We consider this procedure to be valid, since (because of the character of the starting material: mostly hydrated greenschist-facies minerals) we found the reactions to be always very efficient, even at low-temperatures, and phases of unreacted starting material in the experimental results to be almost completely absent (France et al., 2010). This latter observation is something that is often not achieved in partial melting experiments using natural rocks as starting material (for details see Johannes and Koepke, 2001).

France et al. (2010) determined x using least square calculations after the major element compositions of the starting material (= whole rock), and of the phases (93 % of melt at 1030°C; 70 % at 1000°C; 50 % at 970°C; 40 % at 955°C; 27 % at 940°C; 7 % at 910°C; 2 % at 880°C; 1 % at 850°C). Calculated major element compositions of the bulk residual assemblage are reported in Table 1. When partial melting degree decreases (i.e., when temperature decreases from 1030 to 850°C), SiO_2 varies from 36.3 to 54.0 %, MgO varies

from 28.0 to 5.4 wt %, FeO from 23.35 to 10.0 wt %, Al_2O_3 from 1.7 to 16.2 wt %, TiO_2 from 1.0 to 1.5 wt % with a maximum of 2.0 wt % at 1000°C, CaO increases from 7.1 to 12.0 wt % (from 1030°C to 1000°C), and then decreases to 7.8 wt % at 850 °C; Mg# from 68.2 to 49.0 (Figure 4).

The starting material (sample 08OL30) displays rare earth element (REE) concentrations (Table 2) slightly depleted in comparison to N-MORB (0.7 times N-MORB on average; Figure 5, 6). N-MORB normalized trace element contents highlight depletions in Ba, Rb, Nb-Ta, and slightly in Zr-Hf relative to elements of similar incompatibility, and enrichments in Th, U, and Sr (Figure 5, 6). The starting material content in Li, Be, B is 3.85, 0.43, and 7.0 ppm, respectively (Table 3); in comparison, N-MORB average values are 6.1 ppm, 0.64 ppm (Gale et al., 2013), and 0.5 ppm (Chaussidon and Marty, 1995) for Li, Be, and B, respectively. The strong enrichment in B of the starting material relative to N-MORB is consistent with its high grade (greenschist facies) hydrothermal alteration (e.g., Sano et al., 2008).

Trace element contents of the experimental melts have been measured for experimental runs performed between 1030 and 955°C (Figure 5). At lower temperatures (i.e., for lower partial melt fraction) melt-pools were too small (<20μm) to be analyzed with SIMS. With the exception of Sr and V, which display compatible behavior, REE and other trace elements concentrations increase continuously with decreasing degree of partial melting (Figure 5). Li, Be and B contents also increase with decreasing partial melting (from 1.6, 0.35, 5 ppm in 1030°C anatectic melts to 6.1, 0.45, 7.5 ppm, respectively in 955°C melts; Table 3). In comparison to N-MORB (normalized after Gale et al., 2013), a negative Eu anomaly is observed ($Eu/Eu^* = Eu_N/((Sm_N+Gd_N)/2)$), which increases with decreasing partial melting degree from 0.93 to 0.40 (Figure 5). In comparison to the starting material, relative trace element fractionations are generated (Figure 7), including enrichments of U relative to Ba ($U_N/Ba_N = 1.6$ at 955°C), Th ($U_N/Th_N = 1.6$ at 955°C), and Nb ($U_N/Nb_N = 1.2$ at 955°C), Nd relative to Sr ($Nd_N/Sr_N = 2.8$ at 955°C), and Hf relative to Sm ($Hf_N/Sm_N = 1.6$ at 955°C).

In natural settings, the degree of hydrous partial melting is rather low (≤50% in all studied cases on the basis of major element compositions of experimental products and corresponding natural samples; France et al., 2009a; 2010). Trace element concentrations of residual assemblages calculated for the lowest degree of partial melting for which we were able to measure them (at 955°C: 40% melt, 60% residue) using equation (1) are presented in Table 2.

Analytical standard deviations provided for starting material analyses have been considered to calculate minimum and maximum concentrations for the residue (Figure 6). N-MORB normalized compositions of residues are strongly depleted in light REE (LREE), and display a positive Eu anomaly (Eu/Eu*=2.14). The calculated residues are also strongly depleted in High Field Strength Elements (HFSE: Nb, Ta, Zr, Hf) relative to elements of similar incompatibility, and enriched in Sr (Figure 6).

3.2. Natural oceanic rocks

New analyses of dikes and hornfelses from the Oman ophiolite, and of hornfelses from the EPR (IODP Hole 1256D) are presented here (Table 4) together with data from the literature. All information concerning the samples used here, including the source of the data (whether from this study or the literature) is summarized in Table A1. Existing data are EPR dikes and hornfelses from IODP Hole 1256D (Neo et al., 2009; Yamazaki et al., 2009), and plagiogranites sampled at the sheeted dike / gabbro transition in the Oman ophiolite (Pallister and Knight, 1981; Rollinson, 2009).

Dikes from both the Oman ophiolite and the EPR display linear REE N-MORB-normalized patterns ranging from 0.5 to 2 x N-MORB, increasing slightly from LREE to heavy REE (HREE) with La_N/Yb_N=0.6 on average (Figure 6). Trace element contents highlight systematic depletion in Rb relative to Ba and Th, and depletion to enrichment in Ba relative to N-MORB (from 0.3 to 8 x N-MORB). Most of the samples display Eu negative anomalies (with Eu/Eu* down to 0.9), but one Oman sample has Eu/Eu*=1.15. Oman samples display slight negative HFSE anomalies, and EPR samples slight positive anomalies in Nb-Ta.

Hornfelses from Oman ophiolite and from the EPR display strong depletions in LREE (La_N/Sm_N= 0.39 in average) and marked positive Eu anomalies (average Eu/Eu*=1.72 and 1.23 for Oman and EPR samples, respectively) (Figure 6). Patterns are mostly linear and slightly increase from middle REE (MREE) to HREE (average Gd_N/Lu_N= 0.80). All samples display strong Sr positive anomalies, with Sr/Sr* ranging from 1.5 to 8 (with Sr/Sr*=$Sr_N/((Pr_N+Nd_N)/2)$). Samples display Zr depletions relative to elements of similar incompatibility, and to N-MORB. Nb-Ta for EPR hornfelses are depleted relative to N-MORB, but slightly enriched relative to elements of similar incompatibility. Hornfelses from Oman are strongly enriched in Ba relative to Rb (average Ba_N/Rb_N=16).

REE contents of oceanic plagiogranites from Oman ophiolite are up to 3 times higher than N-MORB. Their REE patterns are relatively flat and commonly display Eu negative anomalies. Nb-Ta are depleted and Zr-Hf enriched relative to elements of similar incompatibility; and Ba, Th, and U are strongly enriched relative to Rb.

4. Discussion

The mid-crustal axial melt lens that is normally present at fast-spreading mid-ocean ridges is generally regarded as playing a central role in feeding most of the upper crust (e.g., Sinton and Detrick, 1992; MacLeod and Yaouancq, 2000; Koepke et al., 2011; Wanless and Shaw, 2012) and, to some authors, part of the lower crust also (e.g., Quick and Denlinger, 1993; Henstock et al., 1993; Phipps Morgan and Chen, 1993; Boudier et al., 1996; Nicolas et al., 2009). It is therefore important to understand the range and extent of processes that have the potential to skew the chemical composition of melts within it.

Short length-scale variations in depth to the melt lens along the East Pacific Rise – in places of the order of hundreds of meters vertically over only lateral distances of several kilometers (e.g., Carbotte et al., 2013) – imply that the melt lens migrates up and down on a timescale potentially of decades to centuries (Hooft et al., 1997; Babcock et al., 1998; Gillis and Roberts, 1999; Gillis and Coogan, 2002; France et al., 2009a). This implies a variable local-scale thermal structure, probably related to magma replenishments to the melt lens.

Because hydrous partial melting of altered rocks starts at ~850°C (France et al., 2010), a temperature largely below that of the basaltic magmas believed to fill the melt lens (e.g. Sinton and Detrick, 1992; MacLeod and Yaouancq, 2000; Coogan et al., 2003; Nicolas et al., 2008; Wanless and Shaw, 2012), anatexis is expected to be ubiquitous along fast spreading ridges, at least in the vicinity of the magma chamber roof (provided water is available, which would be the case if dikes are hydrothermally altered). The heat necessary to trigger partial melting could be delivered either by vertical or lateral migrations of the melt lens, or by its inflation due to magma replenishment (e.g., Coogan et al., 2003; France et al., 2009a).

In this study, together with the work of France et al. (2010), we constrain the composition of anatectic melts and associated residual lithologies produced at magma chamber roofs and margins: the environment where hot fresh melts interact with previously hydrothermally

altered country rocks. Here we discuss the presence of residual lithologies at oceanic magma chamber roofs (section 4.1), and the fate of the produced hydrous melts (section 4.2). Finally we attempt to identify chemical markers of melt contamination related to anatectic melts mixing with MORB melts in the melt lens (section 4.3).

Trace element concentrations of products (melt and residue) strongly depend on the protolith composition. All results discussed in the following sections are therefore normalized relative to the likely protolith, *i.e.* to the sheeted dike complex of each studied region, which we consider to be the rocks that formed the initial magma chamber roof (Figure 7).

4.1. Fate of residual assemblages: hornfelsic dikes and enclaves

Investigations of the base of the sheeted dike complex have been conducted in the Troodos and Oman ophiolites (Rothery, 1983; MacLeod and Rothery, 1992; Gillis and Roberts, 1999; Gillis, 2002; Gillis and Coogan, 2002; Gillis, 2008; Nicolas et al., 2008; France et al., 2009a), and at several locations along the EPR (Hess Deep, Pito Deep, ODP Hole 1256D; Wilson et al., 2006; Gillis, 2008; Koepke et al., 2008; France et al., 2009a). In all sites studied the sheeted dike complex root has been extensively recrystallized to hornfelsic assemblages, which differ both petrologically and texturally from normal sheeted dikes. These recrystallized assemblages have been interpreted by previous authors as being formed either through dehydration or by anatexis; in both cases the protolith is considered to be previously hydrothermally altered dike rock.

Trace element contents of all hornfels samples studied herein have been normalized to the sheeted dike composition of the respective studied areas (Figure 7), and the experimental anatectic residue composition has likewise been normalized to the starting material (altered dike) composition.

We find that the experimental residue is depleted in LREE, HFSE (more strongly depleted in Zr-Hf than in Nb-Ta), Ba and Th, and displays positive Eu, and Sr anomalies in comparison to the initial dike (Figure 7). Depletions in HFSE, and positive anomalies in Eu, and Sr clearly reflect the high amount of plagioclase in the residue (Figure 4) as HFSE are strongly incompatible in plagioclase when Eu is weakly incompatible, and Sr compatible (Aigner-Torres et al., 2007; Drouin et al., 2009). These characteristics are also found in the natural

hornfelsic samples from the EPR and from the Oman ophiolite (Figure 7). Similarities between experimentally produced residues and natural hornfels are striking, and support the hypothesis that they result from the same petrogenetic process. Depletions in fluid-immobile elements such as HFSE highlight that dehydration alone cannot explain the depleted trace element patterns: dehydration would not trigger HFSE depletion relative to REE. Anatexis is thus essential to fractionate those elements and thereby produce hornfels (Figure 8). In comparison to experimental residue (generated at a melting degree of 40%), Oman hornfelses display REE patterns that vary from more depleted to similarly depleted (Figure 7b). It shows that partial melting in the Oman natural system probably reached a maximum of 40% but mostly proceeded at lower melting degree. Quartz is commonly present as a late xenomorphic interstitial phase in hornfelsic dikes and enclaves within varitextured gabbros (Koepke et al., 2008; France, 2009; France et al., 2009a), suggesting that silica-rich anatectic melt may be locally trapped within the residual assemblage; a process which may produce trace element-enriched patterns. Hornfelsic enclaves within the isotropic gabbro horizon and close to its transition to underlying foliated gabbros are interpreted as dike root residues that have been stoped into the melt lens and frozen in the act of sinking to its floor (Wilson et al., 2006; France et al., 2009a; Koepke et al., 2011). Elongate lenses of hornfels have also been observed within the underlying vertically foliated gabbros and tentatively related to sheeted dike root assimilation by Boudier et al. (2000), an interpretation consistent with the present study. These observational constraints, together with the modal and chemical correspondence between natural hornfels and experimental residues (generated at partial melting degrees <50%), strongly support the premise that partial anatexis does occur. Total melting and associated full assimilation of generated melts may also occur locally but would leave little evidence.

The occurrence of hornfelsic, partially melted residual lithologies at the base of the sheeted dike complex will affect the physical properties of the upper ocean crust, and may in turn influence the hydrothermal system organization and the melt lens evolution through time. Hornfelses display well-equilibrated textures (e.g., Koepke et al., 2008), and are denser and less porous than altered dikes (Teagle et al., 2006; Violay et al., 2010). The intense fracturing observed in drilled samples at ODP Hole 1256D (e.g., Teagle et al., 2012) is not described in dredged samples (e.g., Gillis, 2008), or in ophiolites (e.g., Coogan et al., 2003; France et al., 2009a), hence we interpret this feature as being related to the drilling process. Because of its inferred low primary permeability, hydrothermal circulation is thus expected to be less

effective in hornfelses than in (less dense and more permeable) altered dikes. Heat transport is assumed to be hampered, operating mainly through conduction, a conclusion also reached by Gillis and Roberts (1999), Coogan et al. (2003) and Gillis (2008) who named this horizon the 'conductive boundary layer' (following Lister, 1974). Consequently, the temperature difference, and the temperature gradient between the top and the bottom of the hornfels horizon tends to decrease; according to a simple thermal flux balance presented by Coogan et al. (2003), the decrease in temperature gradient should in turn result in upward migration of the melt lens and consequent roof assimilation. Anatexis of magma chamber roof may thus proceed and contribute to MORB contamination. This relatively thin conductive boundary layer (i.e. hornfels-dominated horizon) present between the magmatic and hydrothermal convective systems is typically ~100-150 m thick at EPR IODP Site 1256 (Teagle et al., 2012), 25-45 m thick at Pito, and Hess Deep (EPR), and in the Oman ophiolite (Gillis, 2008). At 14°20'S EPR, a 50-60 m thick horizon, effectively the 'magma chamber roof', located just above the melt lens reflector, displays higher Vp than the overlying sheeted dike complex (Singh et al., 1999). Similar Vp differences have been measured between hornfelses and altered dike samples (Violay et al., 2010). Accordingly, we interpret the 'magma chamber roof' identified by Singh et al. (1999) at the EPR as being composed of hornfelses.

In summary, a growing body of evidence indicates that hornfels assemblages produced by hydrous partial melting of previously hydrothermally altered dikes are ubiquitous at roots of fast spreading ridges sheeted dike complexes. The widespread occurrence of hornfelses at magma chamber roofs implies that silica-rich anatectic hydrous melts are regularly generated along mid-ocean ridges. In following sections, we explore the fate of those anatectic melts.

4.2. Fate of anatectic melts: crystallization in situ and mixing

4.2.1. Crystallization *in situ* and genesis of oceanic plagiogranites at the gabbro / dike transition

The anatectic silica-rich melts should be highly viscous ($\eta=10^{4.4}$ Pa.s; France et al., 2010), and can crystallize as intrusive plagiogranites close to the base of sheeted dikes (Figure 1, 2). Such felsic rocks are commonly observed close to oceanic magma chamber roofs in ophiolites and in present-day oceanic crust (e.g. Coleman and Peterman, 1975; Pedersen and Malpas, 1984; Lippard et al., 1986; Coogan et al., 2003; Teagle et al., 2006; Koepke et al., 2008;

Nicolas et al., 2008; France et al., 2010; Grimes et al., 2013). Comparison of plagiogranites selected from two areas of the Oman ophiolite with sheeted dikes from the same areas (Figure 7) highlights that plagiogranites are REE enriched, display negative Eu and Sr anomalies, and enrichments in HFSE, Th, and U. Identical features are observed when comparing the experimental melt formed at 955°C with the starting material (altered dike): the enrichments and depletions are of similar intensities in natural and experimental samples (Figure 7). This direct comparability is therefore consistent with a model in which the studied plagiogranites are generated by anatexis of previously altered dikes.

An alternative model is that the plagiogranites may have been generated by extreme fractionation (e.g., Lippard et al., 1986; Rollinson, 2009; Grimes et al., 2011). Brophy (2008, 2009) showed that the two models could be distinguished on the basis of their REE enrichments (Figure 9a; Brophy, 2009). Brophy (2009) calculated the evolution of the REE content in melts during the fractionation of a MORB basalt (under very oxidizing, and moderately oxidizing conditions; FC2 and FC1 in Figure 9a, respectively), and of an evolved melt obtained after 50 % fractionation of a MORB melt (under very oxidizing conditions; FC3 in Figure 9a). The REE content of melts generated by the hydrous partial melting of a cumulate oceanic gabbro (from the lower oceanic crust) was also modeled (HPM in Figure 9a; Brophy, 2009). The striking similarity between our experimental anatectic melts, and those oceanic plagiogranites from the sheeted dike / gabbro transition, is therefore most consistent with an anatectic origin for the studied oceanic plagiogranites (Figure 9a). It should be noted that the subsequent crystallization that may occur once the anatectic felsic melt is generated could also affect the trace element contents, as could subsequent hydrothermal alteration.

4.2.2. Mixing, and MORB contamination

If not crystallized *in situ* as plagiogranites, anatectic melts formed at magma chamber roofs can mix with mafic liquids present within the melt lens (Figure 1), thereby skewing the chemical compositions of the latter. If the extent of mixing is low, peculiar lithologies may crystallize under high water activities close to magma chamber margins (France et al., 2013), whereas full mixing would led to anatectic melts being entirely diluted within the magma chamber (e.g., Michael and Cornell, 1998; Coogan et al., 2003; Gillis et al., 2003; Wanless et

al., 2011). Based on Cl contents of EPR basalts, Coogan et al. (2003) proposed that 20 % of oceanic crust may be affected by such contamination at crustal levels. A significant contamination component has also been recognized in specific environments using volatile abundances and O isotopes of lavas at the tips of propagating ridge segments (Wanless et al., 2010; 2011), and using low Nb/La in lavas (from 0.6 to 0.9 in contaminated samples) in regions of ridge / hot-spot interaction (Haase et al., 2005). MORB contamination has also been proposed in 'normal ridge settings' (e.g., Michael and Cornell, 1998; Coogan et al., 2003; Le Roux et al., 2006; Cordier et al., 2007) mainly using H_2O concentrations and Cl/Nb ratio. Chlorine and niobium have similar partition coefficients, and the ratio is consequently believed to remain mostly equal to the uncontaminated MORB value (12.5 in Le Roux et al., 2006) when partial or fractional crystallization occurs. Nevertheless, several EPR basalts display higher values (in average 50±7.1) in samples inferred to have been affected by crustal contamination (Le Roux et al., 2006). In all these cases assimilation of anatectic melts appears to have been combined with a significant degree of partial or fractional crystallization of MORB.

In comparing these natural cases with our experimental results, simple concentrations of elements cannot therefore be utilized alone; the potential presence of an anatectic component is instead best detected by looking for incompatible trace element fractionations. Particularly sensitive are Nb depletions relative to REE (Nb/La~0.7 in our experimental melts), and U, Th, Zr, Hf enrichments relative to the starting material and to MORB. The average Cl/Nb value for the anatectic melts presented herein is ~80 and can explain the enrichment in some EPR basalts. It should be noted here that the Cl contents of our anatectic melts represent minimum values, as chlorine may be concentrated in the vapor phase that coexists with the melt.

4.3. How to track MORB contamination?

The aim of this study was not simply to produce another study showing that MORB crustal contamination does indeed occur (e.g., Michael and Schilling, 1989; Chaussidon and Marty, 1995; Michael and Cornell, 1998; Gillis and Coogan, 2002; Coogan, 2003; Coogan et al., 2003; Gillis et al., 2003; Haase et al., 2005; Le Roux et al., 2006; Cordier et al., 2007; France et al., 2009a; Wanless et al., 2010; Wanless et al., 2011; Koepke et al., 2011; Wanless et al., 2012; France et al., 2013), but rather to provide tools to track that contamination. In this study

we present for the first time the major and trace element composition of what we believe to be the principal crustal contaminant of MORB (Tables 1, 2, 3; Figure 7). In order to provide a way to track this crustal contamination component in MORB, we here calculate the global apparent partition coefficients (KD_0) that governed element partitioning during the hydrous partial melting experiments (Equation (2); Figure 9b; Table 5). We suggest that these coefficients will be useful for identifying MORB contamination in future data sets.

$$(2) \quad KD_0 = [concentration]_{residue}/[concentration]_{melt}$$

KD_0 represents the element partitioning between the residual assemblage and the anatectic melt formed at 955°C. The KD_0 values illustrated in Figure 9b have been ordered following the order of decreasing incompatibility during mantle melting (Sun and McDonough, 1989). This ordering allows us to highlight the differences in element behavior (*i.e.*, in KD_0) between the mantle melting process that generated primitive melts, and the anatexis process at the magma chamber roof that can skew MORB signatures. Significant KD_0 positive anomalies are observed for Ba, Th, Sr, Eu, Ti and V relative to neighbor elements, and a Zr-Hf negative anomaly; those anomalies reflect the partition coefficients of elements between the residual minerals and the melt. The compatible behavior ($KD_0>1$) of Sr attests to the large amount of plagioclase in the residue (also consistent with the weak incompatibility of Eu) which also explain the Zr-Hf negative anomalies as these elements are strongly incompatible in plagioclase (Aigner-Torres et al., 2007; Drouin et al., 2009). The compatible behavior of Ti and V attests to the presence of titanomagnetite in the residue. In agreement with estimates based on natural samples (Koepke et al., 2008; France et al.; 2009a, 2010), oxygen fugacity varied in our experiments between FMQ+1.2 and +1.6. It should be noted here that more reducing conditions would result in an enrichment in Ti and V in the anatectic melt as titanomagnetite would be stabilized at lower temperature (lower degree of partial melting). In this case Zr-Hf, and Nb-Ta K_{DS} associated with the anatectic process would be even lower as those elements are relatively enriched in oxides.

Element fractionations presented in section 3.1 can also be used to track the presence of a crustal contamination component in MORB composition. Particularly sensitive are strongly incompatible elements (as Ba, Nb, Ta, Th, Rb…) for which element ratios are believed to remain mostly unchanged during both mantle melting and partial or fractional crystallization processes (e.g., O'Neill and Jenner, 2012). Especially when compared to the starting material composition (Figure 6), anatectic melts are enriched in U relative to Ba, Nb, and Th, in Nd

relative to Sr, and in Hf relative to Sm; more generally, Zr-Hf are enriched relative to LREE, and LREE and MREE are enriched relative to Sr. Depletions in Sr, Ti, V relative to uncontaminated MORB are also expected (Figure 9b). Fractionation of Th relative to U also raises the possibility that contamination at magma chamber roofs may create U-series disequilibria, contributing to the global signal recorded by MORB (Elliott and Spiegelman, 2003).

As previously proposed by Gillis et al. (2003), volatile elements (e.g., boron) can be enriched in MORB through assimilation occurring at magma chamber roofs as hydrothermally altered rocks are boron enriched (e.g., Sano et al., 2008). The hydrothermally altered starting material used in the present study is strongly enriched in boron in comparison to unaltered MORB (Table X); associated anatectic melts are consequently strongly enriched in comparison to N-MORB (up to 15 times). Boron therefore appears to be one of the sensitive proxies to track MORB crustal contamination.

Finally, because it was not possible to analyze the smallest melt pockets present in the low melt fraction experiments, we can expect that the trace element concentrations determined herein for the main MORB crustal contaminant are minimum and maximum values for incompatible and compatible elements, respectively.

5. Conclusion

It is assumed that most of the magmas forming the upper oceanic crust at fast spreading ridges (including MORB) were fed by the small melt lens sandwiched between the top of the main magma chamber below and the sheeted dike complex above (Figure 1). This melt lens is a dynamic horizon that can migrate up, down and / or laterally, with the potential to reheat, melt, and assimilate the previously hydrothermally altered melt lens roof. In the present study, the anatectic processes occurring in that horizon are simulated experimentally. Major and trace element compositions of anatectic melts and residual assemblages are presented and compared with natural samples from the EPR and from the Oman ophiolite.

The residual assemblages of the experiments reproduce the natural hornfelses (dry to hydrous, fine-grained granoblastic gabbronorites) that form the root of the sheeted dike complex, and the experimental anatectic melts reproduce natural oceanic plagiogranites from the dike /

gabbro transition (i.e., at the magma chamber roof). These results provide strong evidence of ongoing anatectic processes at the top of the axial melt lens, and the means to quantify the resulting contamination of MORB melts at fast-spreading mid-ocean ridges.

The process of mixing the anatectic melt with fresh MORB from the melt lens is discussed and the melts are inferred to represent the principal crustal contaminant in MORB. The anatectic melt composition appears to be consistent with the previously identified composition of the inferred crustal contaminant in MORB from the EPR (e.g., Le Roux et al., 2006; Wanless et al., 2010). In comparison to N-MORB, anatectic melt displays enrichment in B, and in Zr-Hf, and depletions in Sr, Ti, V. In comparison to the specific starting material used in the experiments, element fractionations are generated with enrichments in Zr-Hf relative to LREE, in U relative to Ba, Th, and Nb, and in LREE and MREE relative to Sr. The analyzed compositions allow us to calculate global apparent partition coefficients KD_0 between hydrous melts and residues, which can be used to model MORB crustal contamination.

Acknowledgments

References

Aigner-Torres, M., Blundy, J., Ulmer, P., Pettke, T., 2007. Laser ablation ICPMS study of trace element partitioning between plagioclase and basaltic melts: an experimental approach. Contributions to Mineralogy and Petrology 153, 647-667. doi:10.1007/s00410-006-0168-2.

Alt, J.C., Honnorez, J., Laverne, C., Emmermann, R., 1986. Hydrothermal alteration of a 1km section through the upper oceanic crust, deep sea drilling project Hole 504b: Mineralogy, chemistry, and evolution of seawater-basalt interactions. Journal of Geophysical Research 91-B10, 10,309-10,335.

Berndt, J., Koepke, J., Holtz, F., 2005. An experimental investigation of the influence of water and oxygen fugacity on differentiation of MORB at 200 MPa. Journal of Petrology 46, 135-167.

Babcock, J.M., Harding A.J., Kent G.M., Orcutt J.A., 1998. An examination of along-axis variation of magma chamber width and crustal structure on the East Pacific Rise between 13°30′N and 12°20′N. Journal of Geophysical Research 103-B12, 30451-30467. doi:10.1029/98JB01979.

Boudier, F., Nicolas, A., Ildefonse, B., 1996. Magma chambers in the Oman ophiolite: fed from the top and the bottom. Earth and Planetary Science Letters 144, 239-250. doi:10.1016/0012-821X(96)00167-7.

Boudier, F., Godard, M., Armbruster, C., 2000. Significance of gabbronorite occurrence in the crustal section of the Semail ophiolite. Marine Geophysical Research 21, 307-326. doi:10.1023/A:1026726232402

Brophy, J.G., 2008. A study of rare earth element (REE)–SiO2 variations in felsic liquids generated by basalt fractionation and amphibolite melting: a potential test for discriminating between the two different processes. Contributions to Mineralogy and Petrology 156, 337-357. doi:10.1007/s00410-008-0289-x.

Brophy, J.G., 2009. La-SiO2 and Yb-SiO2 systematics in mid-ocean ridge magmas: implications for the origin of oceanic plagiogranite. Contributions to Mineralogy and Petrology 158, 99-111. doi:10.1007/s00410-008-0372-3.

Carbotte, S.M., Marjanovic, M., Carton, H., Mutter, J.C., Canales, J.P., Nedimovic, M.R., Han, S., Perfit, M.R., 2013. Fine-scale segmentation of the crustal magma reservoir beneath the EPR. Nature Geoscience, 6, 866-870, doi:10.1038/NGEO1933

Caress, D.W., Burnett, M.S., 1992. Tomographic image of the axial low-velocity zone at 12°50′N on the East Pacific Rise. Journal of Geophysical Research 97, 9243–9263. doi:10.1029/92JB00287

Carignan, J., Hild, P., Mevelle, G., Morel, J., Yeghicheyan, D., 2001. Routine analyses of trace element in geological samples using flow injection and low pressure on-line liquid chromatography coupled to ICP-MS: a study of geochemical reference materials BR, DR-N, UB-N, AN-G and GH. Geostandards Newsletter 25, 187-198. doi:10.1111/j.1751-908X.2001.tb00595.x

Chaussidon, M., Marty, B., 1995. Primitive boron isotope composition of the mantle. Science 269, 383-386.

Coleman, R.G., Peterman, Z.E., 1975. Oceanic plagiogranite. Journal of Geophysical Research 80, 1099-1108.

Coogan, L.A., 2003. Contaminating the lower crust in the Oman ophiolite. Geology 31-12, 1065-1068.

Coogan, L.A., Mitchell, N.C., O'Hara, M.J., 2003. Roof assimilation at fast spreading ridges: An investigation combining geophysical, geochemical, and field evidence. Journal of Geophysical Research 108-B1, 2002. doi:10.1029/2001JB001171

Cordier, C., Caroff, M., Juteau, T., Fleutelot, C., Hémond, C., Drouin, M., Cotton, J., Bollinger, C., 2007. Bulk-rock geochemistry and plagioclase zoning in lavas exposed along the northern flank of the Western Blanco Depression (Northeast Pacific): Insight into open-system magma chamber processes. Lithos 99, 289-311.

Crawford, W.C., Webb, S.C., Hildebrand, J.A., 1999. Contraints on melt in the lower crust and Moho at the East Pacific Rise, 9°48'N, using seafloor compliance measurements. Journal of Geophysical Research 104-B2, 2923-2939. doi:10.1029/1998JB900087

Detrick, R.S., Buhl, P., Vera, E., Mutter, J., Orcutt, J., Madsen, J., Brocher, T., 1987. Multi-channel seismic imaging of a crustal magma chamber along the East Pacific Rise. Nature 326, 35-41.

Drouin, M., Godard, M., Ildefonse, B., Bruguier, O., Garrido, C.J., 2009. Geochemical and petrographic evidence for magmatic impregnation in the oceanic lithosphere at Atlantis Massif, MAR (IODP Hole U1309D, 30°N). Chemical Geology, 264, 71-88.

Dunn, R.A., Toomey, D.R., Solomon, S.C., 2000. Three-dimensional seismic structure and physical properties of the crust and shallow mantle beneath the East Pacific Rise at 9°30'N. Journal of Geophysical Research 105-B10: 23,537-23,555. doi:10.1029/2000JB900210

Einaudi, F., Godard, M., Pezard, P., Cochemé, J.-J., Brewer, T., Harvey, P., Coulon, C., 2003. Magmatic cycles and formation of the upper oceanic crust at spreading centers: Geochemical study of a continuous extrusive section in the Oman ophiolite. Geochemistry, Geophysics, Geosystems 4, 8608, doi:8610.1029/2002GC000362.

Elliott, T., Spiegelman, M., 2003. 3.14. Melt migration in oceanic crustal production: A U-series perspective. Treatise on Geochemistry 2, The Mantle and Core (ed. Carlson, R.W.) 465-510.

Fahey, A.J., Zinner, E.K., Crozaz, G., Kornacki, A.S., 1987. Microdistributions of Mg isotopes and REE abundances in a Type A calcium-aluminum-rich inclusion from Efremovka. Geochimica et Cosmochimica Acta 51, 3215-3229. doi:10.1016/0016-7037(87)90130-X.

France, L., 2009. Magmatic / hydrothermal interactions at fast spreading mid-ocean ridges: Implications on the dynamics of the axial melt lens. PhD thesis, Géosciences Montpellier, Université de Montpellier II, Montpellier, France; http://tel.archives-ouvertes.fr/tel-00448699

France, L., Nicollet, C., 2010. MetaRep, an extended CMAS 3D program to visualize mafic (CMAS, ACF-S, ACF-N), and pelitic (AFM-K, AFM-S, AKF-S) projections. Computers and Geosciences 36, 786-791. doi:10.1016/j.cageo.2010.01.001

France, L., Ildefonse, B., Koepke, J., 2009a. Interactions between magma and hydrothermal system in Oman ophiolite and in IODP Hole 1256D: Fossilization of a dynamic melt lens at fast spreading ridges. Geochemistry, Geophysics, Geosystems 10-10, .Q10O19. doi: 10.1029/2009GC002652

France, L., Ouillon, N., Chazot, G., Kornprobst, J., Boivin, P., 2009b. CMAS 3D, a new program to visualize and project major elements compositions in the CMAS system. Computers and Geosciences 35, 1304–1310. doi:10.1016/j.cageo.2008.07.002

France, L., Koepke, J., Ildefonse, B., Cichy, S.B., Deschamps, F., 2010. Hydrous partial melting in the sheeted dike complex at fast spreading ridges: experimental and natural observations. Contributions to Mineralogy and Petrology 160-5, 683-704. doi: 10.1007/s00410-010-0502-6

France, L., Ildefonse, B., Koepke, J., 2013. Hydrous magmatism triggered by assimilation of hydrothermally altered rocks in fossil oceanic crust (Northern Oman ophiolite). Geochemistry, Geophysics, Geosystems 14-8, 2598-2614. doi: 10.1002/ggge.20137

Gale, A., Dalton, C.A., Langmuir, C.H., Su, Y., Schilling, J.G., 2013. The mean composition of ocean ridge basalts. Geochemistry, Geophysics, Geosystems, 14, doi:10.1029/2012GC004334.

Gillis, K.M., Roberts, M.D., 1999. Cracking at the magma-hydrothermal transition: Evidence from the Troodos ophiolite, Cyprus. Earth and Planetary Science Letters 169, 227-244. doi:10.1016/S0012-821X(99)00087-4

Gillis, K.M., 2002. The root zone of an ancient hydrothermal system exposed in the Troodos ophiolite, Cyprus. The Journal of Geology 110, 57-74. doi:10.1086/324205

Gillis, K.M., Coogan, L.A., 2002. Anatectic migmatites from the roof of an ocean ridge magma chamber. Journal of Petrology 43, 2075-2095.

Gillis, K.M., Coogan, L.A., Chaussidon, M., 2003. Volatile element (B, Cl, F) behavior in the roof of an axial magma chamber from the East Pacific Rise. Earth and Planetary Science Letters 213, 447-462.

Gillis, K.M., 2008. The roof of an axial magma chamber: A hornfelsic heat exchanger. Geology 36-4, 299-302. doi: 10.1130/G24590A.1.

Grimes, C.B., Ushikubo, T., John, B.E., Valley, J.W., 2011. Uniformly mantle-like $\delta^{18}O$ in zircons from oceanic plagiogranites and gabbros. Contributions to Mineralogy and Petrology 161, 13-33. Doi:10.1007/s00410-010-0519-x

Grimes, C.B., Ushikubo, T., Kozdon, R., Valley, J.W., 2013. Perspectives on the origin of plagiogranite in ophiolites from oxygen isotopes in zircon. Lithos 179, 48-66. doi: 10.1016/j.lithos.2013.07.026

Grove, T.L., Kinzler, R.J., Bryan, W.B., 1992. Fractionation of mid-ocean ridge basalt (MORB). In: Phipps Morgan, J., Blackman, D.K., Sinton, J.M. (Eds.), Mantle Flow and Melt Generation at Mid-Ocean Ridges. American Geophysical Union, Washington DC, pp. 281–310.

Haase, K.M., Stroncik, N.A., Hékinian, R., Stoffers, P., 2005. Nb-depleted andesites from the Pacific-Antarctic Rise as analogs for early continental crust. Geology 33-12, 921-924. doi: 10.1130/G21899.1

Henstock, T.J.,Woods, A.W., White, R.S., 1993. The accretion of oceanic crust by episodic sill intrusion. Journal of Geophysical Research 98 (B3), 4143–4161.

Hofmann, A.W., White, W.M., 1982. Mantle plumes from ancient oceanic crust. Earth and Planetary Science Letters 57, 421-436.

Hooft, E.E.E., Detrick, R.S., Kent, G.M., 1997. Seismic structure and indicators of magma budget along the southern East Pacific Rise. Journal of Geophysical Research 102-B12, 27 319-27 340. doi:10.1029/97JB02349.

Irvine, T.N., Baragar, W.R.A., 1971. A guide to the chemical classification of the common volcanic rocks. Canadian Journal of Earth Sciences 8, 532-548.

Johannes, W., Koepke, J., 2001. Uncomplete reaction of plagioclase in experimental dehydration melting of amphibolite. Australian Journal of Earth Sciences 48, 581-590.

Klein, E.M., 2003. Geochemistry of the Igneous oceanic crust, in Rudnick, R.L., (Eds.), Treatise on Geochemistry Vol. 3, The Crust. Pergamon, pp. 433-463.

Klein, E.M., Langmuir, C.H., 1987. Global correlations of ocean ridge basalt chemistry with axial depth and crustal thickness. Journal of Geophysical Research 92, 8089-8115.

Koepke, J., Berndt, J., Feig, S.T., Holtz, F., 2007. The formation of SiO_2-rich melts within the deep oceanic crust by hydrous partial melting of gabbros. Contributions to Mineralogy and Petrology 153, 67-84. doi : 10.1007/s00410-006-0135-y

Koepke, J., Christie, D.M., Dziony, W., Holtz, F., Lattard, D., Maclennan, J., Park, S., Scheibner, B., Yamasaki, T., Yamazaki, S., 2008. Petrography of the Dike/Gabbro Transition at IODP Site 1256 (Equatorial Pacific): The evolution of the Granoblastic Dikes. Geochemistry, Geophysics, Geosystems 9-7, Q07O09. doi:10.1029/2008GC001939

Koepke, J., France, L., Müller, T., Faure, F., Goetze, N., Dziony, W., Ildefonse, B., 2011. Gabbros from IODP Site 1256, equatorial Pacific: Insight into axial magma chamber processes at fast spreading ocean ridges. Geochemistry Geophysics Geosystems 12-9, Q09014. doi:10.1029/2011GC003655.

Lamoureux, G., Ildefonse, B., Mainprice, D., 1999. Modelling the seismic properties of fast-spreading ridge crustal Low-Velocity Zones: insights from Oman gabbro textures. Tectonophysics 312, 283-301.

Le Roux, P.J., Shirey, S.B., Hauri, E.H., Perfit, M.R., Bender, J.F., 2006. The effects of variable sources, processes and contaminants on the composition of northern EPR MORB (8-10°N and 12-14°N): Evidence from volatiles (H_2O, CO_2, S) and halogens (F, Cl). Earth and Planetary Science Letters 251, 209-231.

Lippard, S.J., Shelton, A.W., Gass, I.G., 1986. The ophiolite of Northern Oman. In: Geological Society Memoir 11, Blackwell, Oxford 178pp.

Lissenberg, C.J., Dick, H.J.B., 2008. Melt-rock reaction in the lower oceanic crust and its implications for the genesis of mid-ocean ridge basalt. Earth and Planetary Science Letters 271, 311-325. doi: 10.1016/j.epsl.2008.04.023

Lissenberg, C.J., MacLeod, C.J., Howard, K.A., Godard, M., 2013. Pervasive reactive melt migration through fast-spreading lower oceanic crust (Hess Deep, equatorial Pacific Ocean). Earth and Planetary Science Letters 361, 436-447.

Lister, C.R.B., 1974. On the penetration of water into hot rocks. Geophysical Journal Of the Royal Astronomical Society, 39, 465-509.

MacLeod, C.J., Rothery, D.A., 1992. Ridge axial segmentation in the Oman ophiolite: evidence from along-strike variations in the sheeted dyke complex. In: Parson, L.M., Murton, B.J. and Browning, P., (eds.) Ophiolites and their Modern Oceanic Analogues. Special Publication of the Geological Society of London 60, 39-63.

MacLeod, C.J., Yaouancq, G., 2000. A fossil melt lens in the Oman ophiolite: Implications for magma chamber processes at fast spreading ridges. Earth and Planetary Science Letters 176, 357-373. doi: 10.1016/S0012-821X(00)00020-0

Marks, N., Schiffman, P., Zierenberg, R. A., 2011. High-grade contact metamorphism in the Reykjanes geothermal system: Implications for fluid-rock interactions at mid-oceanic ridge spreading centers. Geochemistry, Geophysics, Geosystems 12, Q08007. doi:10.1029/2011GC003569.

McDonald, I., Viljoen, K.S., 2006. Platinum-group element geochemistry of mantle eclogites: a reconnaissance study of xenoliths from the Orapa kimberlite, Botswana. Transactions of the Institution of Mining and Metallurgy, Section B: Applied Earth Science 115, 81-93.

Michael, P.J., Cornell, W.C., 1998. Influence of spreading rate and magma supply on crystallization and assimilation beneath mid-ocean ridges: Evidence from chlorine and major element chemistry of mid-ocean ridge basalts. Journal of Geophysical Research 103, 18 325-18 356.

Michael, P.J., Schilling, J.G., 1989. Chlorine in mid-ocean ridge magmas: evidence for assimilation of seawater influenced components. Geochimica et Cosmochimica Acta 53, 3 131-3 143.

Moreira, M., Blusztajn, J., Curtice, J., Hart, S., Dick, H., Kurz, M.D., 2003. He and Ne isotopes in oceanic crust: Implications for noble gas recycling in the mantle. Earth and Planetary Science Letters, 216, 635-643.

Morton, J.L., Sleep, N.H., 1985. Seismic reflections from a Lau basin magma chamber, in: Scholl DW, Vallier TL (Editors), Geology and offshore resources of pacific island arcs-Tonga region. Circum-Pacific Council for Energy and Mineral Resources, Earth Science Series, Houston, Texas, pp. 441-453.

Neo, N., Yamazaki, S., Miyashita, S., 2009. Data report: bulk rock compositions of samples from the IODP Expedition 309/312 sample pool, ODP Hole 1256D, in Teagle, D.A.H., Alt, J.C., Umino, S., Miyashita, S., Banerjee, N.R., Wilson, D.S., and the Expedition 309/312 Scientists, Proc. IODP, 309/312: Washington, DC (Integrated Ocean Drilling Program Management International, Inc.). doi:10.2204/iodp.proc.309312.204.2009

Nicolas, A., Boudier, F., Koepke, J., France, L., Ildefonse, B., Mevel, C., 2008. Root zone of the sheeted dike complex in the Oman ophiolite. Geochemistry, Geophysics, Geosystems 9, Q05001. doi:10.1029/2007GC001918

Nicolas, A., Boudier, F., France, L., 2009. Subsidence in magma chamber and the development of magmatic foliation in Oman ophiolite gabbros. Earth and Planetary Science Letters 284, 76-87. doi: 10.1016/j.epsl.2009.04.012

O'Neill, H.St.C., Jenner, F.E., 2012. The global pattern of trace-element distributions in ocean floor basalts. Nature 491, 698-704. doi:10.1038/nature11678

Pallister, J.S., Knight, R.J., 1981. Rare-Earth Element Geochemistry of the Samail Ophiolite near Ibra, Oman. Journal of Geophysical Research 86-B4, 2673-2697.

Pearce, N.J.G., Perkins, W.T., Westgate, J.A., Gorton, M.P., Jackson, S.E., Neal, C.R., Chenery, S.P., 1997. A compilation of new and published major and trace element data for NIST SRM 610 and NIST SRM 612 glass reference materials. Geostandards Newsletter 21, 115-144.

Pedersen, R.B., 1986. The nature and significance of magma chamber margins in ophiolites: examples from the Norwegian Caledonides. Earth and Planetary Science Letters 77, 100-112.

Pedersen, R.B., Malpas, J., 1984. The origin of oceanic plagiogranites from the Karmoy ophiolite, Western Norway. Contributions to Mineralogy and Petrology 88, 36-52.

Phipps Morgan, J., Chen, Y.J., 1993. The genesis of oceanic crust: magma injection, hydrothermal circulation and crustal flow. Journal of Geophysical Research 98, 6283–6297.

Pouchou, J.L., Pichoir, F., 1991. Quantitative analysis of homogeneous or stratified microvolumes applying the model ''PAP'', in: Heinrich, K.F.J., Newbury, D.E., (Eds.) Electron probe quantification, Plenum Press, New York, pp 31-75.

Quick, J.E., Denlinger, R.P., 1993. Ductile deformation and the origin of layered gabbro in ophiolites. Journal of Geophysical Research 98, 14015-14027.

Reed, W.P., 1992. Certificate of analysis, standard reference materials 610-611. (National Institute of Standard and Technology).

Rollinson, H., 2009. New models for the genesis of plagiogranites in the Oman Ophiolite. Lithos 112, 603-614. doi: 10.1016/j.lithos.2009.06.006

Rothery, D.A., 1983. The base of a sheeted dyke complex, Oman ophiolite: implications for magma chambers at oceanic spreading axes. Journal of the Geological Society of London 140, 287-296.

Rubin, K.H., Sinton, J.M., 2007. Inferences on mid-ocean ridge thermal and magmatic structure from MORB compositions. Earth and Planetary Science Letters 260: 257-276. doi: 10.1016/j.epsl.2007.05.035

Rubin, K.H., Sinton, J.M., Maclennan, J., Hellebrand, E., 2009. Magmatic filtering of mantle compositions at mid-ocean-ridge volcanoes. Nature Geoscience 2, 321-328.

Sano, T., Miyoshi, M., Ingle, S., Banerjee, N.R., Ishimoto, M., Fukuoka, T., 2008. Boron and chlorine contents of upper oceanic crust: Basement samples from IODP Hole 1256D. Geochemistry, Geophysics, Geosystems 9-12, Q12O15. doi:10.1029/2008GC002182

Shimizu, N., Hart, S.R., 1982. Application of the ion microprobe to geochemistry and cosmochemistry. Annual Review Of Earth and Planetary Sciences 10, 483-526.

Singh, S.C., Kent, G.M., Collier, J.S., Harding, A.J., Orcutt, J.A., 1998. Melt to mush variations in crustal magma properties along the ridge crest at the southern East Pacific Rise. Nature 394-6696, 874-878.

Singh, S.C, Collier J.S, Harding, A.J, Kent G.M., Orcutt, J.A, 1999. Seismic evidence for a hydrothermal layer above the solid roof of the axial magma chamber at the southern East Pacific Rise. Geology 27-3, 219-222.

Sinton, J.M., Detrick, R.S., 1992. Mid-ocean ridge magma chambers. Journal of Geophysical Research 97, 197-216. doi:10.1029/91JB02508

Stix, J., Layne, G.D., 1996. Gas saturation and evolution of volatile and light lithophile elements in the Bandelier magma chamber between two caldera-forming eruptions. Journal of Geophysical Research 101, 25 181-25 196.

Sun, S.S, McDonough, W.F., 1989. Chemical and isotopic systematic of oceanic basalts: implications for mantle composition and processes. Special Publications Geological Society London 42, 313-345.

Teagle, D.A.H., Alt, J.C., Umino, S., Miyashita, S., Banerjee, N.R., Wilson, D.S., the Expedition 309/312 Scientists, 2006. Proc. IODP, 309/312. Integrated Ocean Drilling Program Management International, Inc, Washington, DC, doi:10.2204/iodp.proc.309312.

Teagle, D.A.H., Ildefonse, B., Blum, A., Guérin, G., Zakharova, N., Abe, N., Abily, B., Adashi, Y., Alt, J.C., Anma, R., Baines, G., Deans, J., Dick, H., Endo, D., Ferré, E.C., France, L., Godard, M., Harris, M., Kim, Y., Koepke, J.H., Kurz, M.D., Lissenberg, C.J., Miyashita, S., Morris, A., Oizumi, R., Payot, B.D., Python, M., Roy, P., Till, J.L., Tominaga, M., Wilson, D.S., 2012. Proc. IODP, 335: Tokyo (Integrated Ocean Drilling Program Management International, Inc.). doi: 10.2204/iodp.proc.335.2012.

Violay, M., Pezard, P.A., Ildefonse, B., Belghoul, A., Laverne, C., 2010. Petrophysical properties of the root zone of the sheeted dikes in the ocean crust: A case study from Hole ODP/IODP 1256D, Eastern Equatorial Pacific. Tectonophysics 493, 139-152.

Wanless, V.D., Shaw, A.M., 2012. Lower crustal crystallization and melt evolution at mid-ocean ridges. Nature Geoscience 5, 651-655. doi:10.1038/NGEO1552.

Wanless, V.D., Perfit, M.R., Ridley, W.I., Klein, E.E.E., 2010. Dacite petrogenesis on mid-ocean ridges: Evidence for oceanic crustal melting and assimilation. Journal of Petrology 51, 2377-2410. doi:10.1093/petrology/egq056.

Wanless, V.D., Perfit, M.R., Ridley, W.I., Wallace, P.J., Grimes, C.B., Klein, E.M., 2011. Volatile abundances and oxygen isotopes in basaltic to dacitic lavas on mid-ocean ridges: The role of assimilation at spreading centers. Chemical Geology 287, 1-2, 54-65.

Wanless, V.D., Perfit, M.R., Klein, E.M., White, S., Ridley, W.I., 2012. Reconciling geochemical and geophysical observations of magma supply and melt distribution at the 9°N overlapping spreading center, East Pacific Rise. Geochemistry, Geophysics, Geosystems 13-11, Q11005. doi:10.1029/2012GC004168.

Wilson, D.S., Teagle, D.A.H., Alt, J.C., Banerjee, N.R., Umino, S., Miyashita, S., Acton, G.D., Anma, R., Barr, S.R., Belghoul, A., Carlut, J., Christie, D.M., Coggon, R.M., Cooper, K.M., Cordier, C., Crispini, L., Durand, S.R., Einaudi, F., Galli, L., Gao, Y., Geldmacher, J., Gilbert, L.A., Hayman, N.W., Herrero-Bervera, E., Hirano, N., Holter, S., Ingle, S., Jiang, S., Kalberkamp, U., Kerneklian, M., Koepke, J., Laverne, C., Vasquez, H.L.L., Maclennan, J., Morgan, S., Neo, N., Nichols, H.J., Park, S.H., Reichow, M.K., Sakuyama, T., Sano, T., Sandwell, R., Scheibner, B., Smith-Duque, C.E., Swift, S.A., Tartarotti, P., Tikku, A.A., Tominaga, M., Veloso, E.A., Yamasaki, T., Yamazaki, S., Ziegler, C., 2006. Drilling to gabbro in intact ocean crust. Science 312, 1016-1020. doi: 10.1126/science.1126090

Yamazaki, S., Neo, N., Miyashita, S., 2009. Data report: whole-rock major and trace ele- ments and mineral compositions of the sheeted dike–gabbro transition in ODP Hole 1256D, in Teagle, D.A.H., Alt, J.C., Umino, S., Miyashita, S., Banerjee, N.R., Wilson, D.S., and the Expedition 309/312 Scientists, Proc. IODP, 309/312: Washington, DC (Integrated Ocean Drilling Program Management International, Inc.). doi:10.2204/ iodp.proc.309312.203.2009

Figure captions:

Figure 1: Schematic cross axis view of the magmatic system at fast spreading ridges (modified after France et al., 2009). From top to bottom, crust is composed of extrusives and dikes (forming the upper crust), varitextured gabbros, vertically foliated gabbros, and horizontally layered gabbros (forming the lower crust). The main magma chamber is composed of a mush containing less than 20% of melt, topped by a melt lens that is dominated by melt. Dashed blue curves identify hydrothermal circulation. The insert focuses on the melt lens roof where MORB melts may be contaminated through assimilation of anatectic melts. Red dots indicate the residual hornfelsic assemblages, salmon colored areas with '+' are plagiogranite intrusions, and pink areas highlight melt lens contamination.

Figure 2: a) Outcrop in the Oman ophiolite showing oceanic plagiogranites (felsic, white rocks) intruding the base of the sheeted dike complex (dark rocks). The dike-xenoliths and the sheeted dike complex base are recrystallized to granoblastic textures (hornfels). Wadi Rajmi, in the northern Oman ophiolite. **b)** Microphotographs of an IODP Hole 1256D hornfels composed of plagioclase, clinopyroxene, orthopyroxene and oxides (sample 234R-1_7-9; plane-polarized light).

Figure 3: Triangular projections; a) Alkaline (Na_2O+K_2O)-FeO_{total}-MgO discriminating diagram for tholeiitic and calc-alkaline series from Irvine and Baragar (1971); b) SiO_2/50-TiO_2-K_2O discriminating ternary plot for plagiogranites origin. The different fields are derived from Figure 10 in France et al. (2010). Projection is done using a modification of the program of France et al. (2009b), and France and Nicollet (2010).

Figure 4: Modal proportions of experiments, and major element composition (in wt %) of experimental melt and residue as a function of the degree of partial melting (F% from 0 to 100%); data from France et al. (2010). Shaded area represents the compositional range of primitive MORB (variation is related to spreading rate), from Rubin and Sinton (2007).

Figure 5: N-MORB normalized REE and trace elements contents of starting material and experimental melts (normalization values from Gale et al., 2013). Blue triangles: starting material; black circles: 1030°C experiment melts (melt fraction = 0.93); green circles: 1000°C experiment melts (0.70); red circles: 970°C experiment melts (0.50); yellow circles: 955°C experiment melts (0.40%).

Figure 6: N-MORB normalized REE and trace elements contents of (a) EPR and Oman dikes (starting material composition is added for comparison), (b) experimental melt formed at 955°C (averaged value), and related calculated residue composition (see below), (c) Oman plagiogranites and hornfelses, and (d) IODP Hole 1256D hornfelses. In (b) residual assemblage composition has been calculated for the experiment with the lowest degree of partial melting (at 955°C) using equation (1), compositions are presented in Table 2. Analytical standard deviations provided for starting material analyses have been considered in order to calculate the minimum and maximum possible concentrations for residue. Normalization values are from Gale et al. (2013). * = samples taken from literature (see Table A1 for details). In all graphs dashed lines represent extrapolated values.

Figure 7: REE and trace element compositions of (a) experimental products (955°C) compared (normalized) to the starting material composition, and (b and c) natural plagiogranites and hornfelses compared (normalized) to the regional dikes. Samples from Oman are presented in (b), and samples from IODP Hole 1256D are presented in (c). In (b) and (c), experimental melts and residue compositions are reported for comparison (same symbols as in (a)). * = samples taken from literature (see Table A1 for details). In all graphs dashed lines represent extrapolated values.

Figure 8: K_2O versus Zr concentrations in Oman, 1256D, and experimental hornfelses normalized (subscript 'initial') to the respective protoliths (Oman altered dikes, IODP Hole 1256D altered dikes, and experimental starting material). A value equal to 1 highlights no variation relative to the protoliths. When considering the residue, the partial melting process is expected to reduce the concentration in incompatible elements (such as K and Zr), while

dehydration is expected to reduce the concentration of fluid-mobile elements (such as K), and the fluid-immobile elements (such as HFSE, e.g., Zr) remain unchanged. A slight increase in Zr is expected when the dehydration degree increases since other elements are leached. Natural samples from the Oman ophiolite, and from the EPR are similar to the experimental products, and clearly point to a magmatic process (anatexis) rather than pure dehydration.

Figure 9: (a) Cl/C_0 for La concentrations versus SiO_2 (wt %) for experimental melts (labeled 'this study'), and different processes modeled by Brophy (2009). Processes modeled are: (FC1) the fractionation of a MORB basalt under moderately oxidizing conditions (QFM), (FC2) the fractionation of a MORB basalt under very oxidizing (QFM+3.5), (FC3) the fractionation of an evolved melt obtained after 50 % of fractionation of a MORB melt under very oxidizing conditions (QFM+3.5), and (HPM) the hydrous partial melting of a cumulative oceanic gabbro (from the bottom of oceanic crust). Oceanic plagiogranites sampled in the Oman ophiolite close to the sheeted dike complex / gabbro transition presented in this study are added for comparison together with data from Lippard et al. (1986). (b) Calculated global apparent partition coefficients obtained for the 955°C experiment using equation (2). Elements are ordered following the order of decreasing incompatibility during mantle melting (Sun and McDonough, 1989) to highlight anomalies created by assimilation of anatectic melts.

Table 1: Melt and residue major element compositions expressed in weight %. Residue compositions are calculated using equation (1). Chlorine is expressed in ppm, temperature in °C, and F represent the melt fraction varying between 0 and 1. All compositions are normalized to 100.

Table 2: Trace element compositions expressed in ppm for experimental melts and for the calculated residue (at 955°C). A minimum and a maximum value for the residue are calculated using the starting material composition, the analytical error, and the melt composition and proportion. AVG = average, SD = standard deviation.

Table 3: Li-Be-B concentrations in experimental melts, and the starting material, expressed in ppm. SD = standard deviation, n = number of analyses. MORB average values are also indicated. Li and Be concentrations are from Gale et al. (2013) and B concentration from Chaussidon and Marty (1995).

Table 4: Natural samples major (in weight %) and trace (in ppm) element compositions.

Table 5: Calculated apparent global partition coefficients (KD_0) for the anatectic process. * highlights values extrapolated.

Table A1: Samples used in the present study. IODP sample names (a) represent: site, hole, core, top (in cm), data origin (b): [1] this study; [2] Neo et al. (2009); [3] Yamazaki et al. (2009); [4] Pallister and Knight (1981); [5] Rollinson, (2009); [6] France et al. (2010); * highlights hornfelses sampled as xenoliths hosted in the uppermost isotropic, varitextured gabbros. UTM coordinates are indicated for new samples from the Oman ophiolite.
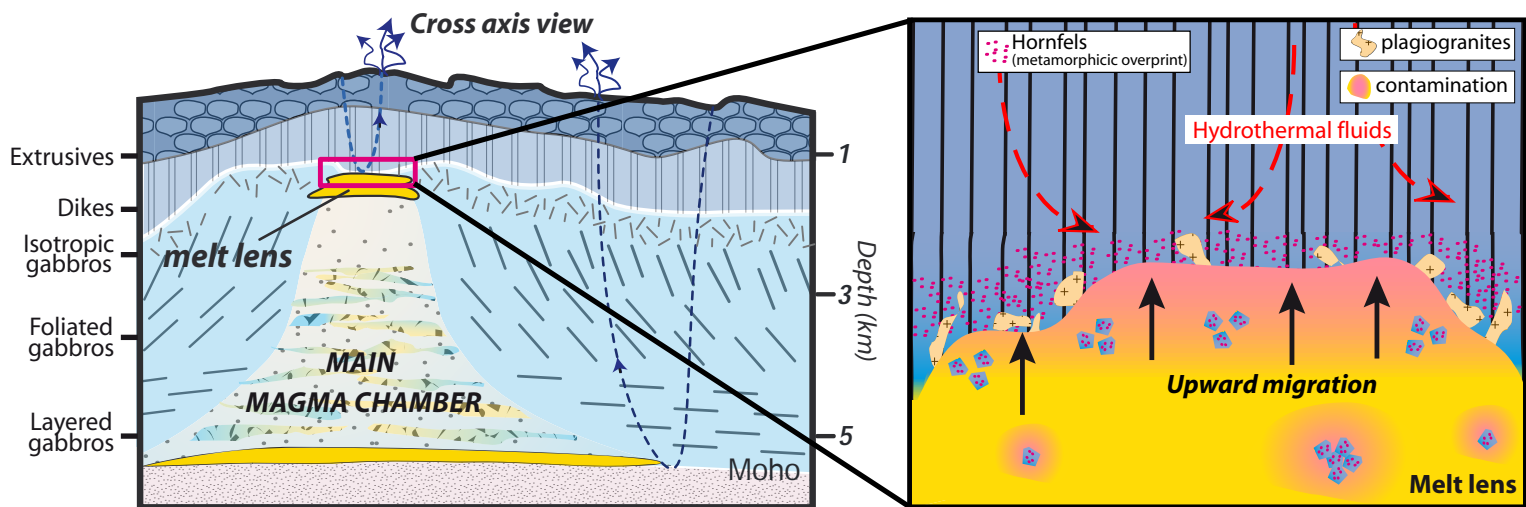
MORB contamination at crustal levels

Trace element partitionning during the process:

Graphical abstract
France et al.,
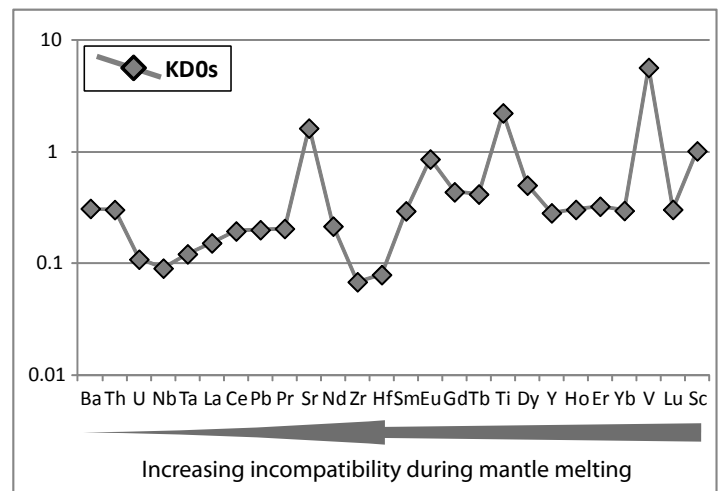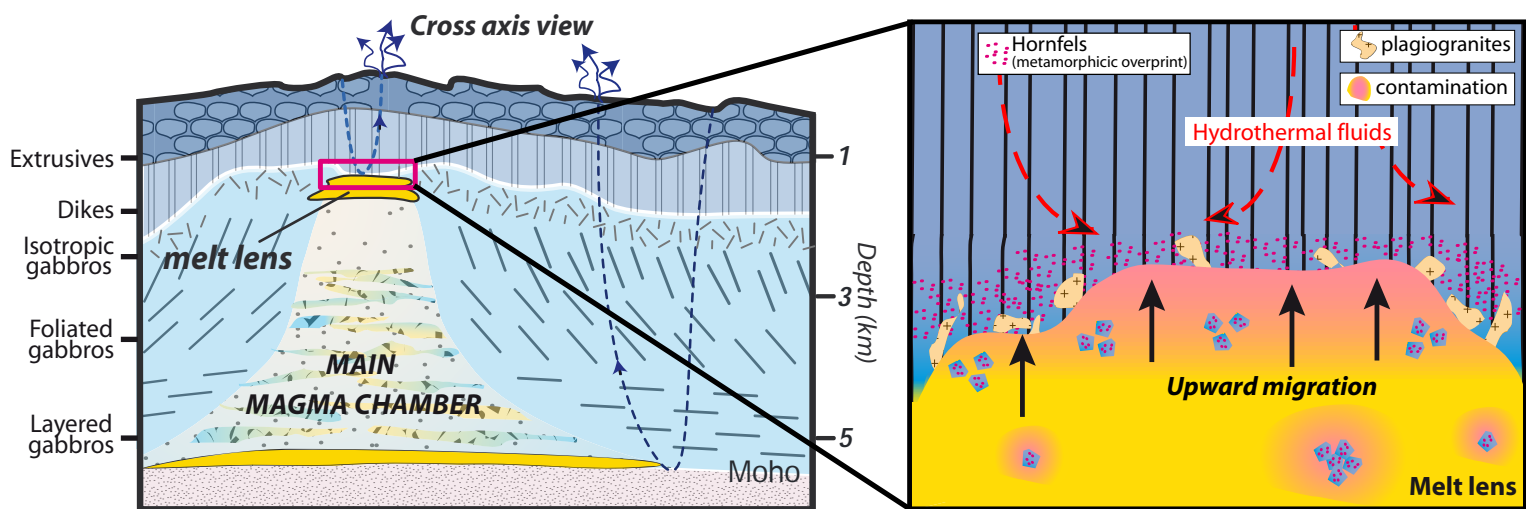
Figure 1
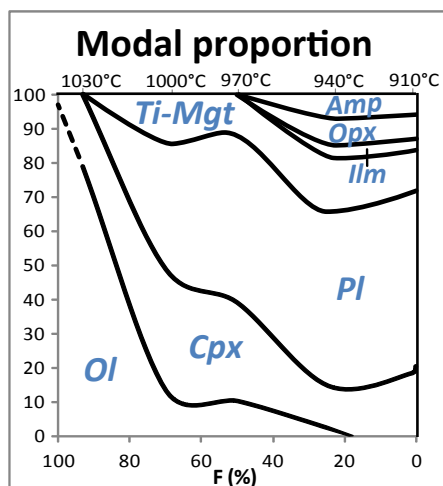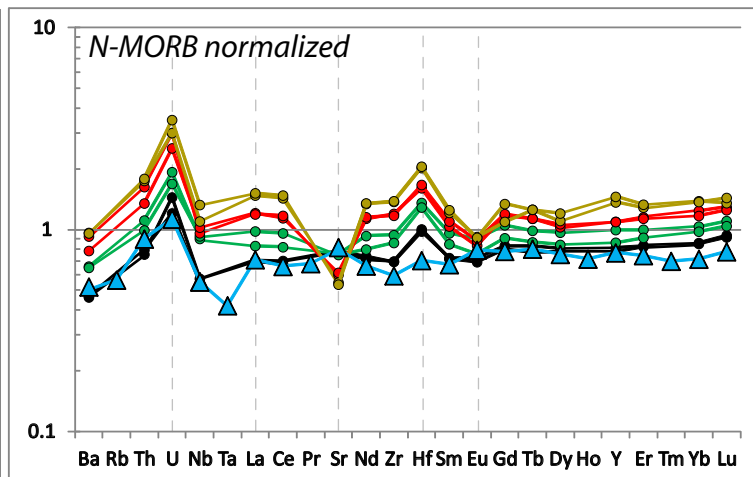France et al.,
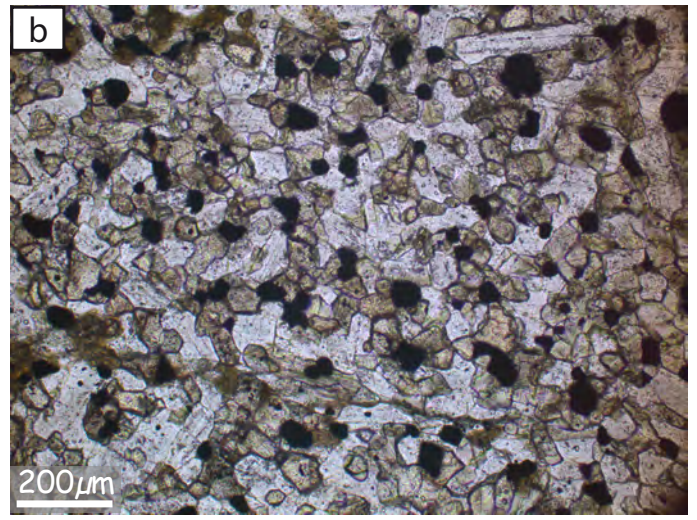
Figure 2
France et al.,
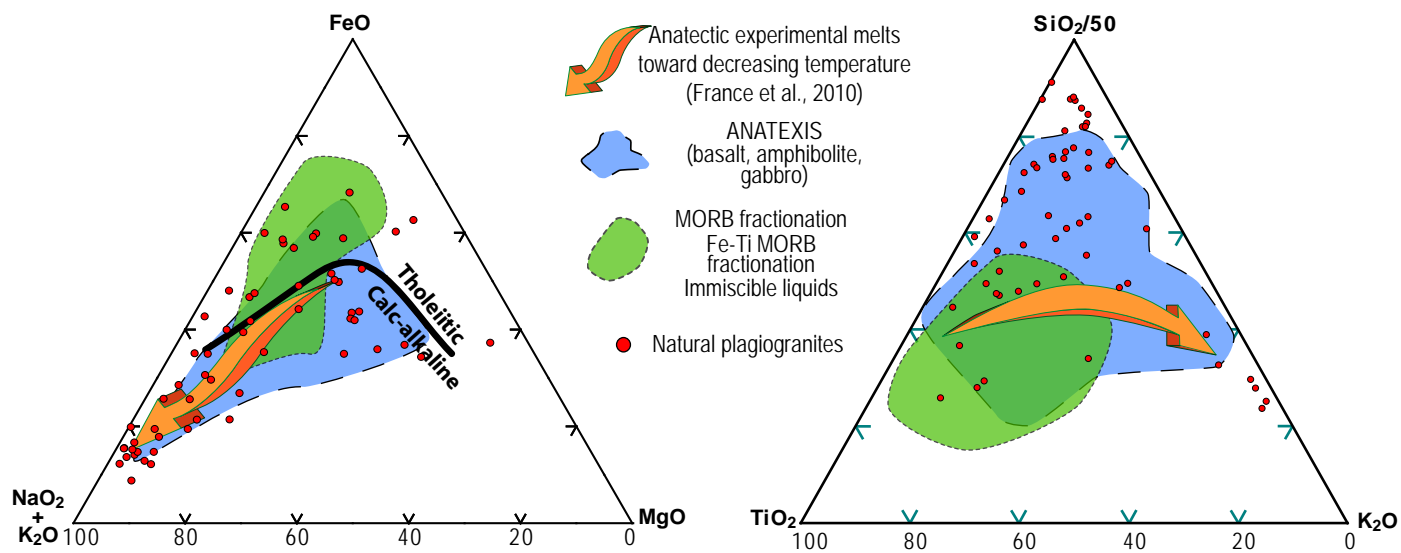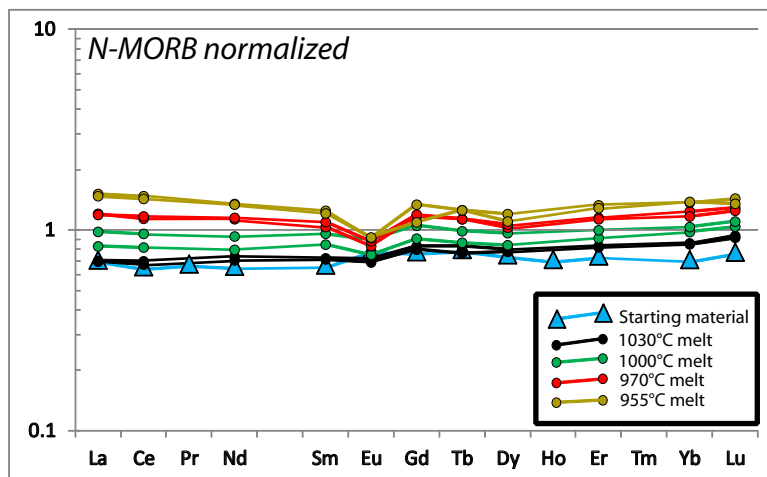
Figure 3
France et al.,
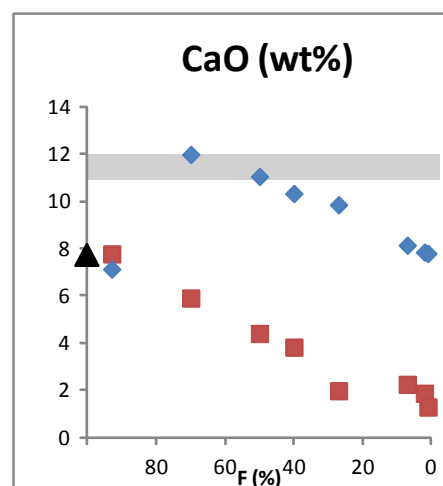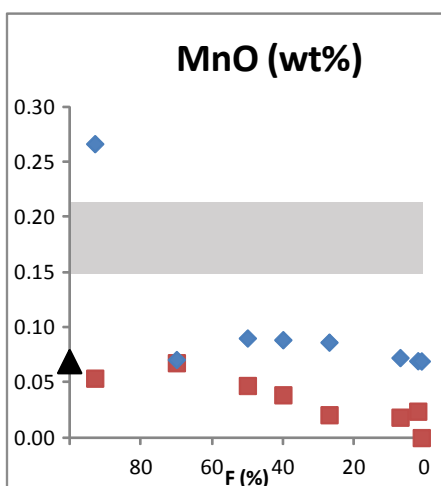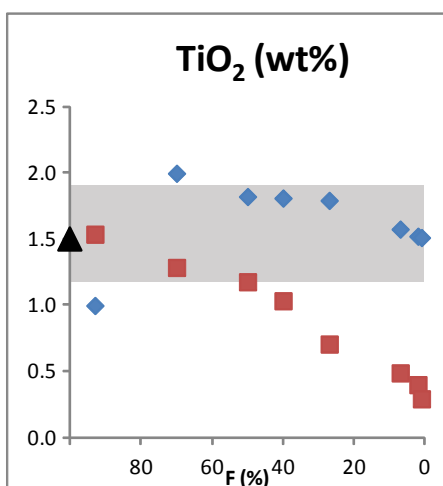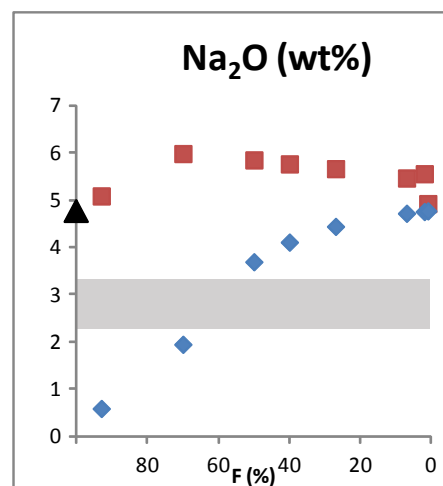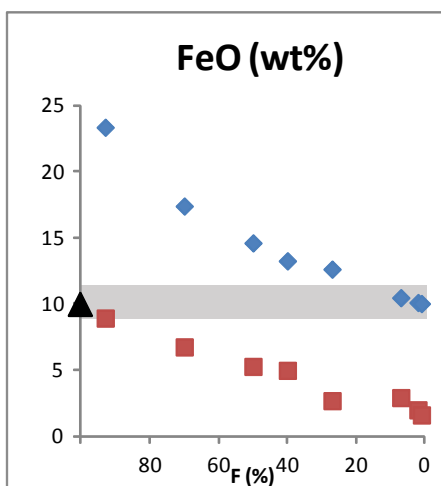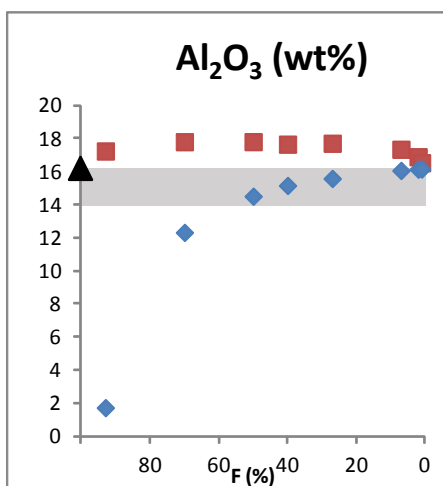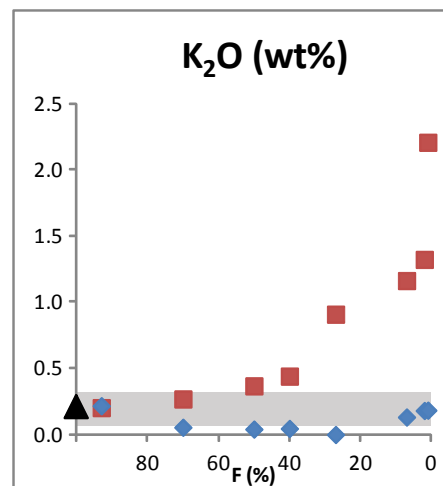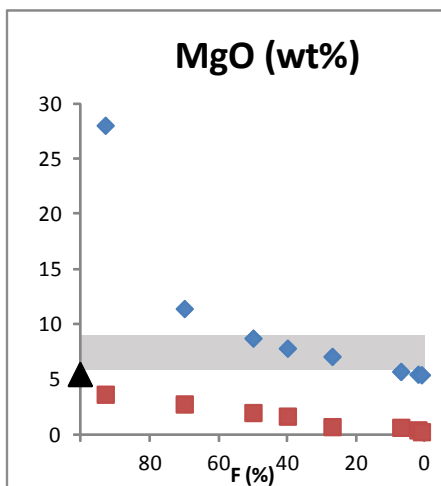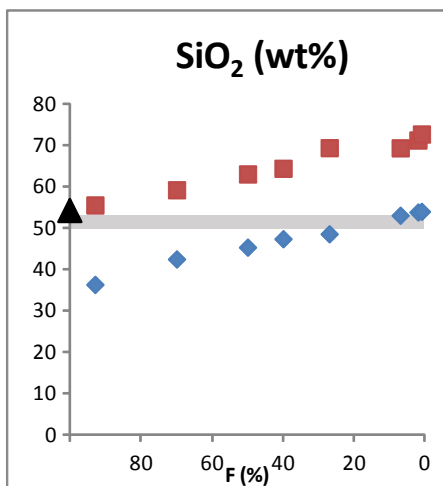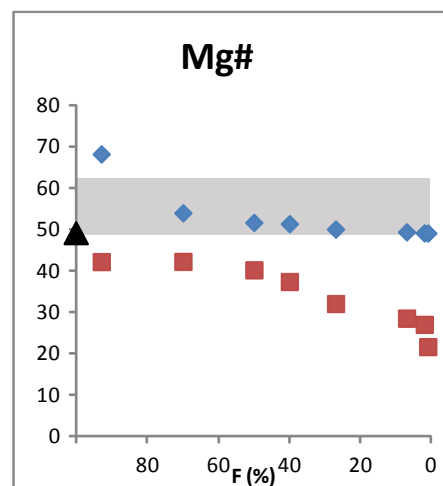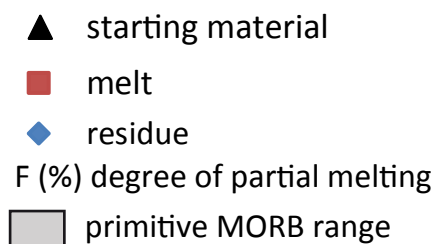
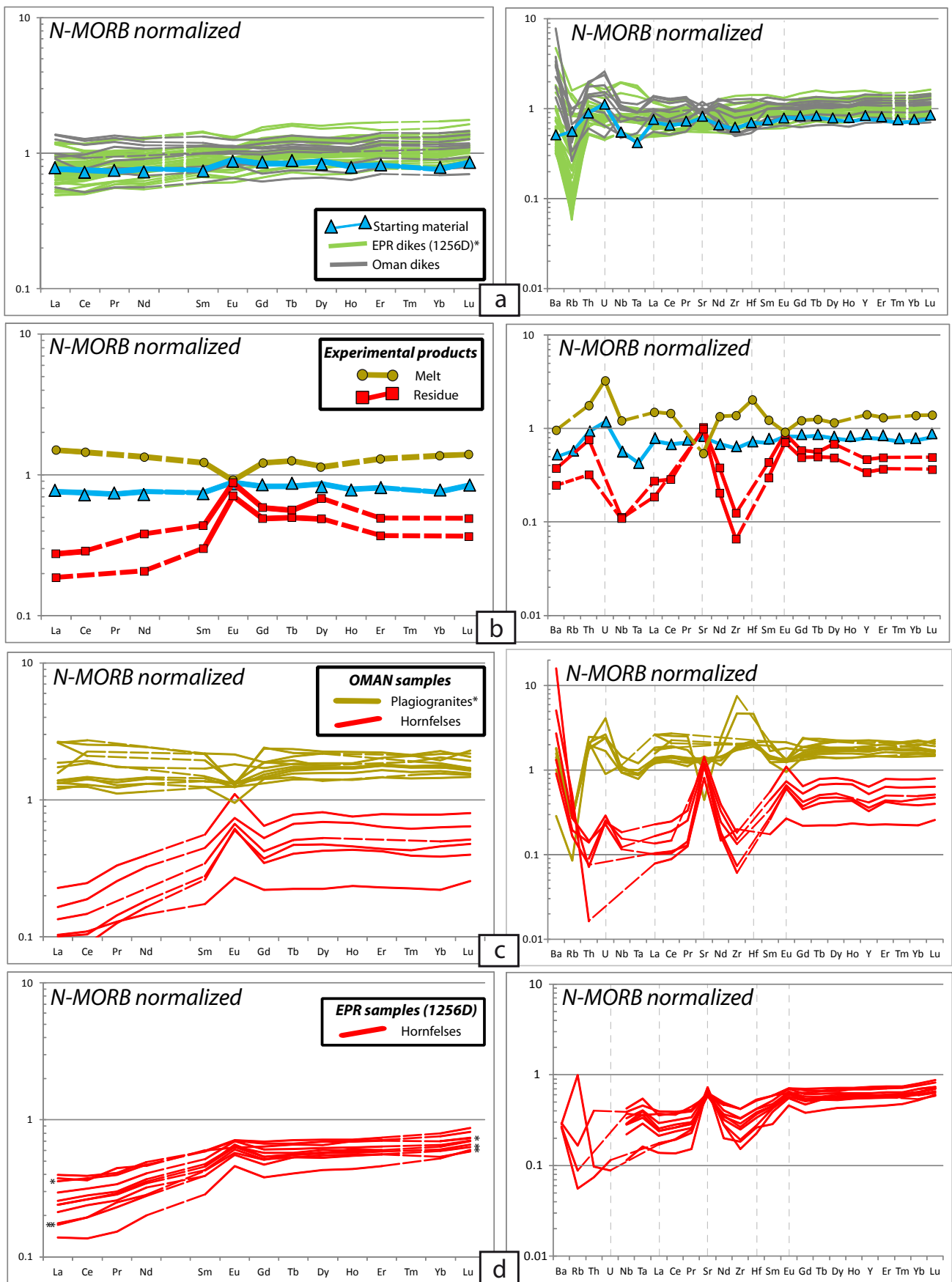France et al., Figure 4

Figure 5
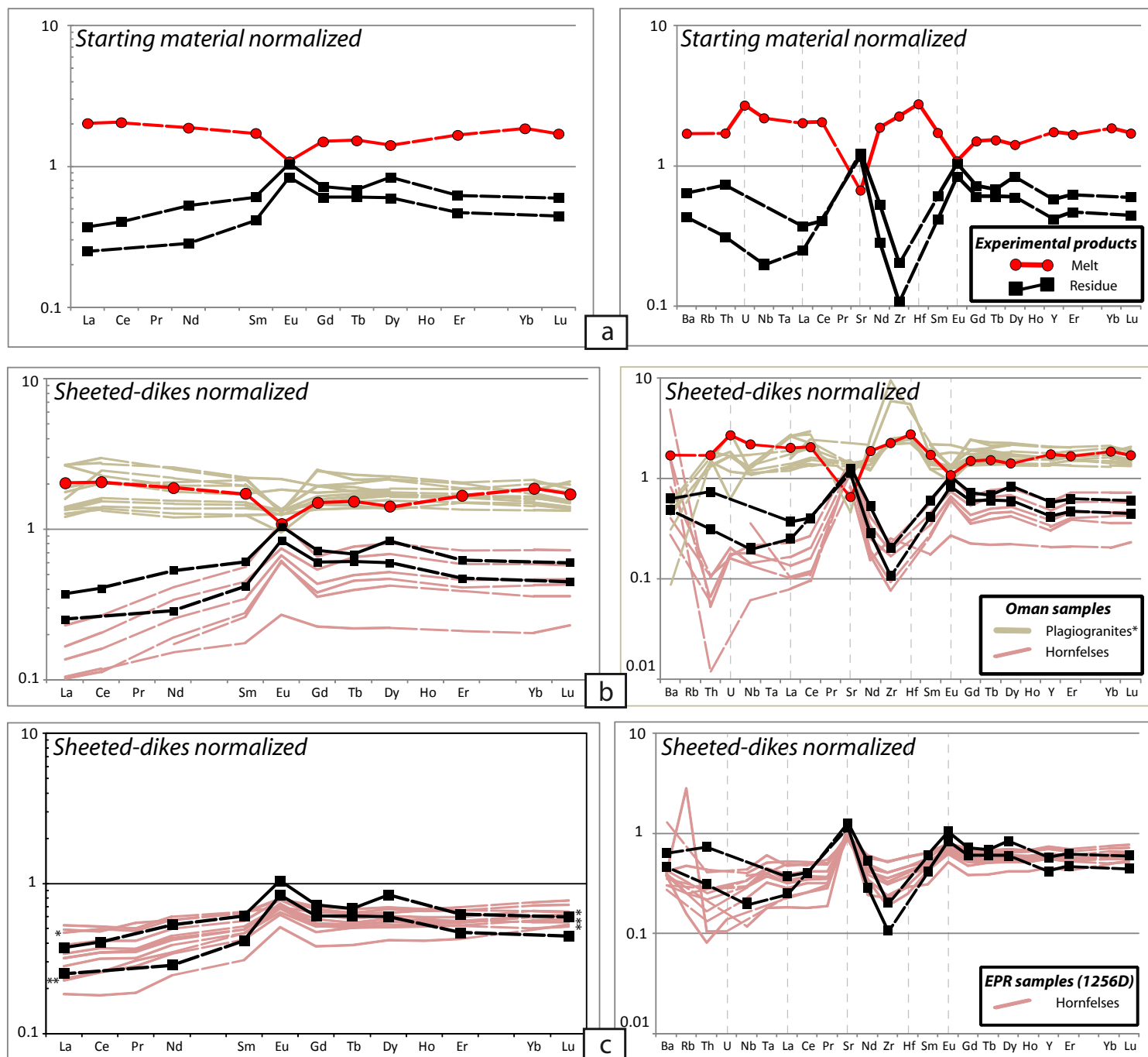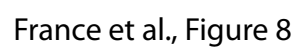France et al.,

Figure 6
France et al.,

Figure 7
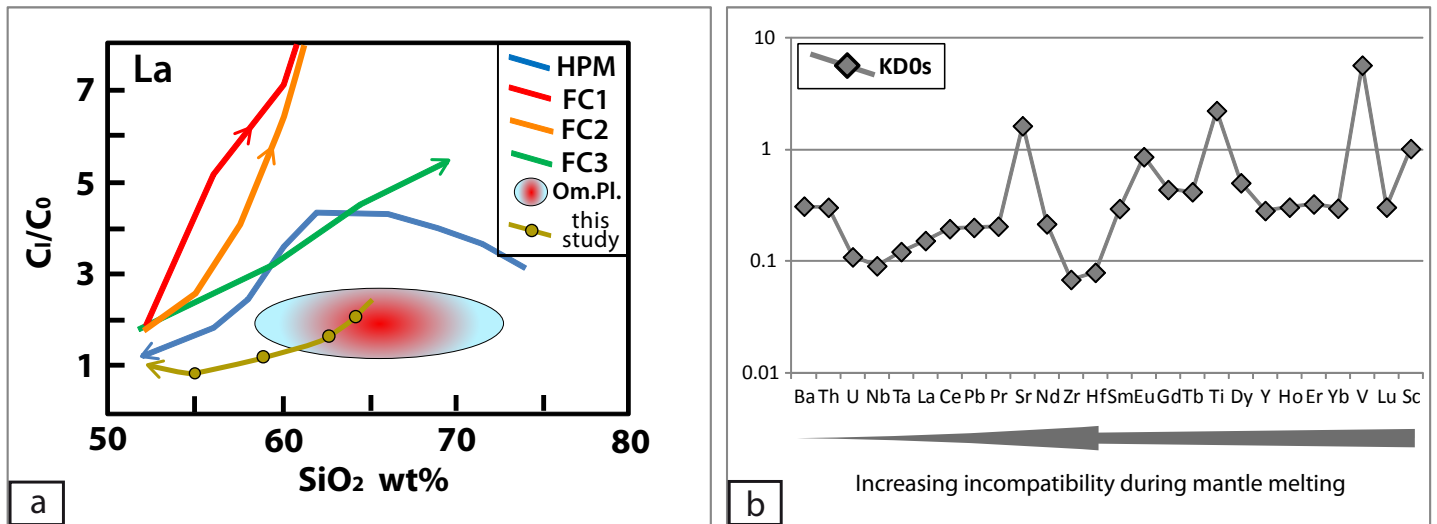France et al.,

France et al., Figure 8

Figure 9
France et al.